Sterile neutrino hot, warm, and cold dark matter

Kevork Abazajian,* George M. Fuller,† and Mitesh Patel‡
Department of Physics, University of California, San Diego, La Jolla, California 92093-0319

(Dated: January 30, 2001)

We calculate the incoherent resonant and non-resonant scattering production of sterile neutrinos in the early universe. We find ranges of sterile neutrino masses, vacuum mixing angles, and initial lepton numbers which allow these species to constitute viable hot, warm, and cold dark matter (HDM, WDM, CDM) candidates which meet observational constraints. The constraints considered here include energy loss in core collapse supernovae, energy density limits at big bang nucleosynthesis, and those stemming from sterile neutrino decay: limits from observed cosmic microwave background anisotropies, diffuse extragalactic background radiation, and ^{6}Li/D overproduction. Our calculations explicitly include matter effects, both effective mixing angle suppression and enhancement (MSW resonance), as well as quantum damping. We for the first time properly include all finite temperature effects, dilution resulting from the annihilation or disappearance of relativistic degrees of freedom, and the scattering-rate-enhancing effects of particle-antiparticle pairs (muons, tauons, quarks) at high temperature in the early universe.

PACS numbers: 95.35.+d,14.60.Pq,14.60.St,98.65.-r

I. INTRODUCTION

In this paper we calculate the non-equilibrium resonant and non-resonant production of sterile neutrinos in the early universe and describe cosmological and astrophysical constraints on this dark matter candidate. Depending on their masses and energy distributions, the sterile neutrinos so produced can be either cold, warm, or hot dark matter (CDM, WDM, HDM, respectively) and may help solve some contemporary problems in cosmic structure formation. We can define sterile neutrinos generically as spin-1/2, $SU(2)$-singlet particles which interact with the standard $SU(2)$-doublet ("active") neutrinos ν_e, ν_μ, and ν_τ, solely via ordinary mass terms. Singlet neutrinos with masses $\sim 10^{12}$ GeV arise naturally, for example, in "see-saw" models of neutrino mass in grand unified theories (GUTs) [1]. Recent solar, atmospheric, and accelerator neutrino oscillation experiments [2–6]), however, imply the existence of four light neutrino species with masses $\lesssim 10\,\mathrm{eV}$, only three of which can be active, on account of limits on the invisible decay width of the Z^0 boson [7]. The remaining neutrino must be sterile. The existence of multiple generations of quarks and leptons in the standard model (SM) of particle physics, as well as many independently-motivated extensions of the SM, imply that there are additional, more massive sterile neutrinos with couplings to active neutrinos currently beyond direct experimental reach. We describe herein the cosmological implications of these heavier sterile neutrinos.

Some early constraints on massive sterile neutrino production in the early universe were derived in Refs. [8, 9]. The first analytical estimates of the relic sterile neutrino abundance from scattering-induced conversion of active neutrinos were made by Dodelson and Widrow [10]. They assumed a negligible primordial lepton number, or asymmetry, so the neutrinos are produced non-resonantly. They found that sterile neutrinos could be a WDM candidate with interesting consequences for galactic and large scale structure. A process that can create sterile neutrino dark matter with a unique energy distribution was proposed by Shi and Fuller [11]. In that work a non-vanishing initial primordial lepton number gives rise to mass-level crossings which enhance sterile neutrino production, yielding dark matter with an energy spectrum which is grossly non-thermal and skewed toward low energies. In particular, the average energy is significantly less than that of an active neutrino, and the neutrinos suppress structure formation on small scales and behave like CDM on large scales (*i.e.*, they behave as WDM or "cool DM").

At no previous time has there been a greater need for a more comprehensive study of the cosmological and astrophysical consequences of active-sterile neutrino mixing. The continuing influx of data from neutrino experiments and new observations of galaxy cores and clusters demand a more detailed understanding of the physics of sterile neutrino dark matter production and more sophisticated calculations of their relic abundances.

We examine these experimental and observational issues in Secs. II and III, respectively. In Sec. IV we discuss

*Electronic address: kabazajian@ucsd.edu
†Electronic address: gfuller@ucsd.edu
‡Electronic address: mitesh@physics.ucsd.edu

the present limits on primordial lepton asymmetries and possible dynamical origins of these asymmetries. We attempt to unify the perspectives of previous work, so we take the initial lepton asymmetry of the universe to be a free parameter within the rather generous bounds set by experiment. After reviewing the physics of neutrino oscillations and matter-affected neutrino transformation in Sec. V, we compute the consequences of pre-existing lepton asymmetries for sterile neutrino dark matter scenarios in Secs. VI and VII. In Sec. VI, we give the Boltzmann equations governing the non-equilibrium conversion of active neutrinos into sterile neutrinos and solve them in the limit of non-resonant conversion, a limit which obtains when the lepton asymmetry is sufficiently small, of order the baryon asymmetry. In Sec. VII, we consider larger asymmetries and examine in detail the physics of resonant neutrino transformation in the early universe. For the non-resonant and several resonant cases we display contours of constant relic density of sterile neutrinos in the plane of neutrino mixing parameters. These results confirm and extend previous work [10, 11]. For both sets of calculations we also take into account finite-temperature and finite-density effects for all three active neutrino species; the dilution of sterile neutrino densities due to heating of the photons and active neutrinos from the annihilation of particle-antiparticle pairs before, during, and after the quark-hadron (QCD) transition, and we allow for the enhanced active neutrino scattering rates due to the increased number of scatterers in equilibrium at high temperatures. In Sec. VIII we calculate the collisionless damping scales relevant for structure formation, scales which classify the regions of dark matter parameter space as HDM, WDM, or CDM regions. We consider in Sec. IX the limits on sterile neutrino dark matter from the diffuse extragalactic background radiation (DEBRA), cosmic microwave background (CMB), big bang nucleosynthesis (BBN), and ^{6}Li and D photoproduction. Finally, in Sec. X we examine the implications of active-sterile neutrino mixing in core-collapse (Type Ib/c, II) supernovae. Conclusions are given in Sec. XI. Throughout the paper we use natural units with $\hbar = c = k_B = 1$.

II. NEUTRINO ANOMALIES

Recent experiments have provided data indicating evidence for new neutrino physics. The most significant recent evidence is the Super-Kamiokande Collaboration's statistically convincing result [2], verifying previous measurements [3], of a suppression of the atmospheric $\nu_\mu/\bar{\nu}_\mu$ flux. The most persuasive Super-Kamiokande evidence for neutrino oscillations is the measured zenith angle dependence of the $\nu_\mu/\bar{\nu}_\mu$ flux, an observation fit most simply by maximal $\nu_\mu \rightleftharpoons \nu_\tau$ mixing in vacuum, with vacuum mass-squared difference $\delta m^2 \sim 3 \times 10^{-3}\,\mathrm{eV}^2$.

On another front, the ground-breaking observations by the Homestake Collaboration found a solar neutrino flux far below that predicted on the basis of sophisticated solar models [4]. The solar neutrino problem has an interesting possible solution through matter-enhanced resonant conversion via the Mikheyev-Smirnov-Wolfenstein (MSW) mechanism [12] or through vacuum or "quasi-vacuum" oscillations [13]. Depending on whether the solar solution involves two-, three-, or four-neutrino mixing, the parameter space of neutrino mass-squared difference and vacuum mixing angle are constrained differently [5].

A third indication for neutrino oscillations comes from the Los Alamos Liquid Scintillator Neutrino Detector (LSND) Collaboration's observations of excess ν_e and $\bar{\nu}_e$ events in beams of ν_μ and $\bar{\nu}_\mu$, respectively. These have been interpreted as evidence for neutrino oscillations in the $\nu_\mu \to \nu_e$ and $\bar{\nu}_\mu \to \bar{\nu}_e$ channels [6]. The Karlsruhe Rutherford Medium Energy Neutrino (KARMEN) experiment probes the same channels but does not see evidence for neutrino oscillations [14]. A joint analysis of the LSND and KARMEN data has found that there are regions of neutrino mixing parameter space consistent with both experiments' results [15].

Efforts have been made to embed the above neutrino oscillation solutions within a three-neutrino framework [16–19]. Leaving aside maximal vacuum mixing of all three neutrino species [16], these analyses generally require the atmospheric neutrino oscillation length scale to be the one associated with the short-base-line LSND experiment [17, 18], or the solar and atmospheric solutions must be built on the same mass difference scale [19].

However, the zenith-angle dependence of the Super-Kamiokande measurement requires the atmospheric neutrino oscillation length to be much larger than the corresponding LSND scale [2, 6]. This disfavors the first three-neutrino scheme. Additionally, the three solar neutrino experimental modes presently available suggest an energy dependence in the ν_e survival probability which is likely inconsistent with the second three-neutrino scheme. Taking these two length scales, and the results of global flux measurement fits for the solar neutrino oscillation interpretation [5], the three different oscillation length and energy scales require three disparate mass differences, which cannot be accommodated in a three-neutrino framework. The CERN e^+e^- collider LEP measurement of the Z^0 width indicates the number of active neutrinos with masses $< m_Z/2$ is 3.00 ± 0.06 [7], so the results are *prima facie* evidence for a light sterile neutrino species.

A number of neutrino mass models can provide the masses and mixings needed to accommodate all of the neutrino oscillation data [20–25]. For example, in some string theories, higher-dimensional operators, suppressed by the powers of the ratio of some intermediate mass scale and the string scale, can give the light and comparable Dirac and Majorana masses necessary for appreciable active-sterile neutrino mixing [20]. In theories with light composite fermions, several of the fermions may mix with standard model neutrinos, giving light active and sterile neutrinos [21]. In the minimal supersymmetric standard model (MSSM) with explicit R-parity violation, a neutralino can provide the required mixing for the atmospheric and solar neutrino problems [22, 23]. This model can also supply a sterile or "weaker-than-weakly" interacting particle that has a small mixing with one or more active neutrino flavors. A low-energy extension of the Standard Model with an $SO(3)$ gauge group acting as a "shadow sector" may result in a neutral heavy lepton [24]. A model with several sterile neutrino dark matter "particles" arises in brane-world scenarios. It invokes bulk singlet fermions coupling with active neutrinos on our brane [25]. However, many models of bulk neutrinos as sterile neutrino dark matter must be rather finely tuned and must avoid several cosmological constraints [26].

Although these mass models have been proposed to account for the existing neutrino anomalies, many of them already contain or can be easily be extended to contain additional singlet states which also mix with active neutrinos. As long as the new particles are sufficiently massive and have sufficiently small mixings with active neutrinos, they evade terrestrial constraints, and it is interesting and useful to speculate on their cosmological and astrophysical consequences. As we show later in this paper, even apparently negligible active-sterile neutrino mixing is sufficient to induce the production of sterile neutrino dark matter in the early universe.

A specific model's viability in producing a sterile neutrino dark matter candidate depends on whether the mass and mixing properties of the candidate(s) with the active neutrinos lie within the range that produces an appropriate amount of dark matter, and whether the candidate is stable over the lifetime of the universe, does not engender conflicts with observationally-inferred primordial light element abundances, does not violate CMB bounds, and does not contribute excessively to the DEBRA in photons [27]. Potential constraints on these scenarios also may arise from deleterious effects associated with the neutrino physics of core-collapse (Type Ib/c, II) supernovae (see, *e.g.*, Refs. [28–30] and Sec. X). Constraints on massive sterile neutrinos ($10\,\mathrm{MeV} \leq m_s \leq 100\,\mathrm{MeV}$) from the SN 1987A signal and BBN were considered previously in Ref. [31].

The existence of massive sterile singlet neutrinos that mix with ν_e has been probed in precision measurements of the energy spectrum of positrons in the pion decay $\pi^+ \to e^+\,\nu_e$. The best current limits are from Britton *et al.*, [32], which constrain the mixing matrix element $|U_{ex}|^2 < 10^{-7}$ for sterile neutrino masses $50\,\mathrm{MeV} < m_s < 130\,\mathrm{MeV}$. These limits may be significantly improved in future precision experiments [33]. Less stringent constraints from peak and kink searches exist for smaller m_s. In addition, searches for decay of massive ν_s have yielded constraints for $|U_{\mu x}|^2$, $|U_{\tau x}|^2$ [34], as well as $|U_{ex}|^2$ [7].

III. STRUCTURE FORMATION

Conflicts may have appeared between standard cold dark matter theory and simulations and observations of large and small scale cosmological structure. Simulations predict about 500 small halos (*i.e.*, dwarf galaxies) with mass greater than $10^8\,M_\odot$ around a galaxy like the Milky Way, but only 11 candidates are observed near the Milky Way [35], and only 30 in the local group out to $\sim$1.5 Mpc [36]. In other words, simulations of the standard Λ-CDM model *may* predict more dwarf galaxies than are seen (but see Ref. [37]). Also, even if the dwarf halos are dark, their overabundance may hinder galactic disk formation [38].

Another potential problem with CDM simulations is the appearance of singularities or "cusps" of high density in the cores of halos. The observations of the innermost profiles of galaxy clusters are ambiguous [39], but rotation curves of the central regions of dark matter-dominated galaxies consistently imply low inner densities [40]. Recent N-body calculations of the nonlinear clustering of WDM models have found that enhanced collisionless damping can lower halo concentrations, increase core radii, and produce far fewer low mass satellites [41]. Also, the observed phase space density in dwarf spheroidal galaxies may suggest a primordial velocity dispersion like that of WDM [42].

A promising new constraint on the nature of dark matter may come from study of the Lyα forest in the spectrum of high-redshift quasars [43, 44]. The structure of the Lyα forest at high redshifts has been used to constrain the contribution of HDM and, therefore, the mass of the active neutrinos [45]. The constraints presented in Ref. [45] and the Gerstein-Zeldovich–Cowsik-McLelland bound [46] only pertain to fully populated active neutrino seas with a thermal energy spectrum. For example, if an active neutrino has a mass $m_{\nu_\alpha} \sim 1\,\mathrm{keV}$ ($\alpha = \mu, \tau$) and the reheating temperature of inflation is low ($T_{\mathrm{RH}} \sim 1\,\mathrm{MeV}$), then the corresponding active neutrino sea will not be fully populated [47, 48] and can be WDM [49]. However, observations of the power spectrum of the Lyα forest cannot only constrain HDM scenarios, but also may be able to test the viability of WDM scenarios. Since the absolute normalization of the power spectrum is uncertain, the relative presence of power between scales near $\sim 1\,\mathrm{Mpc}$ and near $\sim 100\,\mathrm{kpc}$ may constrain the WDM scenarios that have a relatively large contrast in power between these scales [50]. In addition, the large number of high-redshift quasars found by the Sloan Digital Sky Survey (SDSS) [51] can add considerably to the knowledge of the Lyα power spectrum, particularly at the largest scales. The combination of the galactic power spectrum from SDSS and the Lyα power spectrum will produce even stronger constraints on the behavior of dark matter on small scales.

IV. PRIMORDIAL LEPTON ASYMMETRY

The lepton number or asymmetry of a neutrino flavor α is defined to be

$$L_\alpha \equiv \frac{n_{\nu_\alpha} - n_{\bar{\nu}_\alpha}}{n_\gamma}, \tag{4.1}$$

where n_{ν_α} is the proper number density of neutrino species ν_α, and $n_\gamma = 2\zeta(3)T^3/\pi^2 \approx 0.243T^3$ is the proper number density of photons at temperature T. The lepton number(s) of the universe is (are) not well constrained by observation. The best limits come from the energy density present during BBN and the epoch of decoupling of the CMB [52–55]. In fact, the best current bounds on the lepton numbers come from the observational limits on the ^{4}He abundance, radiation density present at the CMB decoupling, and structure formation considerations [52, 54, 55]:

$$-4.1 \times 10^{-2} \leq L_{\nu_e} \leq 0.79, \tag{4.2}$$

$$|L_{\nu_\mu,\nu_\tau}| \leq 6.0. \tag{4.3}$$

The bound on positive L_{ν_e} is weaker than that for negative L_{ν_e} since it is possible to combine the effects of neutron-to-proton ratio (n/p) reduction of positive L_{ν_e} with a large L_{ν_μ} or L_{ν_τ}, which increases the expansion rate and thus the n/p ratio entering BBN. This cancellation could provide a neutrino "degenerate" BBN that could replicate not only the primordial ^{4}He, but also the D/H and ^{7}Li abundances predicted by standard BBN. See Refs. [52, 54] for a further discussion. As stated, the limits (4.2), (4.3) depend on an assumption of a roughly Fermi-Dirac, low-chemical-potential energy spectrum for each neutrino species. They do not address neutrino mass and do not take account of potential bounds stemming from closure (*i.e.*, age of the universe) considerations. The above limits do not change significantly when recent estimates of observationally-inferred primordial abundances are employed [54]. In any case, it is clear that neutrino number density asymmetries less than about 10% of the photon number are easily allowed. However, we will see that lepton asymmetries at this level, or even several orders of magnitude smaller, could have a significant and constrainable effect if there are massive sterile neutrinos (see Sec. VII).

An issue which arises whenever the lepton number(s) L_{ν_α} differ from the baryon number B (or $\eta = n_b/n_\gamma \approx 2.79 \times 10^{-8}\Omega_b h^2 \sim 10^{-10}$, where n_b is the proper baryon number density and Ω_b is the baryon rest mass closure fraction and h is the Hubble parameter in units of $100\,\mathrm{km\,s^{-1}\,Mpc^{-1}}$) concerns the process of baryogenesis. For example, electroweak baryogenesis predicts the equality of these numbers $B - L = 0$. Note that there also exist simple processes that violate $B - L$ and create lepton and/or baryon number either through the Affleck-Dine mechanism [56] or through non-equilibrium decays of a heavy Majorana particle [57]. In Ref. [58], several natural scenarios of producing a large lepton number and the observed small baryon number were investigated. Furthermore, lepton number could arise spontaneously through matter-enhanced active-sterile neutrino transformation at energy scales below that of the baryogenesis epoch [59, 60]. Finally, it should be recognized that through cancellation of lepton numbers we could have $B - L = 0$ (where $L = L_{\nu_e} + L_{\nu_\mu} + L_{\nu_\tau}$), while still having significant lepton-driven weak potentials [see Eq. (5.12)] in the early universe.

V. MATTER-AFFECTED NEUTRINO TRANSFORMATION

A. General framework

Neutrino mixing phenomena arise from the non-coincidence of energy-propagation eigenstate and the weak (interaction) eigenstate bases. Eigenstates of neutrino interaction (flavor) include the active neutrinos (ν_e, ν_μ, ν_τ) which are created and destroyed in the standard model weak interactions, as well as sterile neutrinos (*e.g.*, ν_s, ν_s', ν_s'', ...) which do not participate in weak interactions. Eigenstates of neutrino propagation are states of definite mass and energy (or momentum) and evolve independently of each other between weak interaction vertices. If the bases spanned by these sets of eigenstates happen to coincide, then active and sterile neutrinos propagate independently between interactions. In general, however, the bases need not coincide, since the symmetries of the standard model and its many proposed extensions do not require the unitary transformation between the bases to be the identity transformation. As a result, neutrinos can oscillate, or transform in flavor, between interactions.

This physics applies for any number of neutrino flavors, including the four (three active plus one sterile) which can accommodate the neutrino experiments. In the environments we consider, active-active mixing is suppressed due to the very similar matter effects for all active species. In general, the 4-neutrino evolution may have multiple active species mixing with the sterile neutrino, or in multiple-sterile scenarios, there may be mixing between the sterile neutrinos. In our analysis here, we consider the simplifying limit of two neutrino (active-sterile) mixing to explore the basic physics of sterile neutrino dark matter production.

In the case of two-neutrino mixing, the unitary transformation between the bases can be written as

$$\begin{aligned}|\nu_\alpha\rangle &= \cos\theta|\nu_1\rangle + \sin\theta|\nu_2\rangle\\ |\nu_s\rangle &= -\sin\theta|\nu_1\rangle + \cos\theta|\nu_2\rangle\end{aligned}$$

where $|\nu_\alpha\rangle$ and $|\nu_s\rangle$ are active ($\alpha = e, \mu, \tau$) and sterile neutrino flavor eigenstates, respectively, and $|\nu_1\rangle$ and $|\nu_2\rangle$ are neutrino mass (energy) eigenstates with mass eigenvalues m_1 and m_2, respectively. The vacuum mixing angle θ parametrizes the magnitude of the mixing (and, as we shall see, the effective coupling of the sterile neutrino in vacuum). We choose all of the neutrino flavor and mass eigenstates to be eigenstates of momentum with eigenvalue p. Then a mass-energy eigenstate $|\nu_i\rangle$ ($i = 1, 2$) develops in time and space with the phase

$$e^{i\vec{p}_i\cdot\vec{x}} = e^{i(\mathbf{p}\cdot\mathbf{x}-E_i t)} = e^{i(px-\sqrt{m_i^2+p^2}t)} \approx e^{-ixm_i^2/2p}, \tag{5.1}$$

where $E_i = \sqrt{m_i^2+p^2}$ is the energy of the eigenstate; $p \equiv |\mathbf{p}|$ is the magnitude of the proper momentum of the species. If the neutrino mass eigenstates are relativistic so that $E_i \gg m_i$, we have $E_i \approx p + m_i^2/2p$ and $x \approx t$, yielding the last approximation in Eq. (5.1). (In this last approximation we suppress the part of the evolution operator proportional to the trace, as this simply gives an overall common phase to the states.) In our study of sterile neutrino production, the sterile neutrinos are always relativistic during the epochs in which they were produced.

The difference of the squares of the vacuum neutrino mass eigenvalues is, for example, $\delta m^2 = m_2^2 - m_1^2$. We can follow the evolution of a coherently propagating neutrino state $|\Psi_\nu\rangle$ in either the mass-energy or flavor basis. In the flavor basis, a Schrödinger-like equation describes how the flavor amplitudes, $a_\alpha(x) = \langle\nu_\alpha|\Psi_\nu(x)\rangle$ with $\alpha = e, \mu, \tau$ and $a_s(x) = \langle\nu_s|\Psi_\nu(x)\rangle$, develop with time-space coordinate x:

$$i\frac{d}{dx}\begin{pmatrix} a_\alpha \\ a_s \end{pmatrix} = \left\{\left(p + \frac{m_1^2+m_2^2}{4p} + \frac{V(x,p)}{2}\right) I + \frac{1}{2}\begin{pmatrix} V(x,p) - \Delta(p)\cos 2\theta & \Delta(p)\sin 2\theta \\ \Delta(p)\sin 2\theta & \Delta(p)\cos 2\theta - V(x,p)\end{pmatrix}\right\}\begin{pmatrix} a_\alpha \\ a_s \end{pmatrix}, \tag{5.2}$$

where the first term is proportional to the identity and $\Delta(p) \equiv \delta m^2/2p$. In the context of the early universe it is most convenient to take $x = t$, the Friedman-Lemaitre-Robertson-Walker coordinate time (age of the universe), while in supernovae we take x to be position. The weak potential $V(x,p)$ represents the effects of neutrino neutral current and charged current forward scattering on particles in the plasma carrying weak charge. In the early universe we have $V(T,p)$, but in supernovae, V also depends on position x. We suppress the x and T dependence of V in the rest of the paper. For a review of these issues and neutrino astrophysics, see, *e.g.*, Refs. [61–64].

Neutrino mixing can be modified by the presence of a finite temperature background and any asymmetry in lepton number. The oscillation length is

$$l_m = \left\{\Delta^2(p)\sin^2 2\theta + \left[\Delta(p)\cos 2\theta - V^D - V^T(p)\right]^2\right\}^{-1/2}. \tag{5.3}$$

The effective matter-mixing angle is

$$\sin^2 2\theta_m = \frac{\Delta^2(p)\sin^2 2\theta}{\Delta^2(p)\sin^2 2\theta + [\Delta(p)\cos 2\theta - V^D - V^T(p)]^2}. \tag{5.4}$$

Matter effects have been separated into finite density and finite temperature potentials, V^D and $V^T(p)$.

The finite density potential V^D arises from *asymmetries* in weakly interacting particles (*i.e*, nonzero lepton numbers), not from non-zero total densities alone. In general, the finite density potential is [64, 65]

$$V^D = \begin{cases} \sqrt{2}G_F\left[2(n_{\nu_e} - n_{\bar\nu_e}) + (n_{\nu_\mu} - n_{\bar\nu_\mu}) + (n_{\nu_\tau} - n_{\bar\nu_\tau}) + (n_{e^-} - n_{e^+}) - n_n/2\right] & \text{for } \nu_e \rightleftharpoons \nu_s, \\ \sqrt{2}G_F\left[(n_{\nu_e} - n_{\bar\nu_e}) + 2(n_{\nu_\mu} - n_{\bar\nu_\mu}) + (n_{\nu_\tau} - n_{\bar\nu_\tau}) - n_n/2\right] & \text{for } \nu_\mu \rightleftharpoons \nu_s, \\ \sqrt{2}G_F\left[(n_{\nu_e} - n_{\bar\nu_e}) + (n_{\nu_\mu} - n_{\bar\nu_\mu}) + 2(n_{\nu_\tau} - n_{\bar\nu_\tau}) - n_n/2\right] & \text{for } \nu_\tau \rightleftharpoons \nu_s. \end{cases} \tag{5.5}$$

The thermal potential V^T arises from finite temperature effects and neutrino forward scattering on the seas of thermally created particles [64]:

$$V^T(p) = -\frac{8\sqrt{2}G_F p_\nu}{3m_Z^2}\left(\langle E_{\nu_\alpha}\rangle n_{\nu_\alpha} + \langle E_{\bar\nu_\alpha}\rangle n_{\bar\nu_\alpha}\right)$$

$$-\ \frac{8\sqrt{2}G_{\rm F}p_\nu}{3m_{\rm W}^2}\left(\langle E_\alpha\rangle n_\alpha + \langle E_{\bar\alpha}\rangle n_{\bar\alpha}\right), \quad (5.6)$$

where n_α ($n_{\bar\alpha}$) is the proper number density of leptons (anti-leptons) of flavor α and $\langle E_\alpha\rangle$ ($\langle E_{\bar\alpha}\rangle$) is the average energy of the lepton (antilepton), and n_{ν_α} ($n_{\bar\nu_\alpha}$) and $\langle E_{\nu_\alpha}\rangle$ ($\langle E_{\bar\nu_\alpha}\rangle$) are the proper number density and average energy of the neutrinos (antineutrinos) of flavor α. The second term in Eq. (5.6) must be included whenever the lepton of the same flavor as the active neutrino in question is populated.

In this paper, we will assume that the *initial* neutrino distribution functions are close to Fermi-Dirac black bodies, which for occupation of differential interval dp have the form

$$\begin{aligned} dn_{\nu_\alpha} &\approx \frac{n_{\nu_\alpha}}{T^3F_2\left(\eta_{\nu_\alpha}\right)}\frac{p^2dp}{e^{E(p)/T-\eta_{\nu_\alpha}}+1} \\ &\approx \left(\frac{n_\gamma}{4T^3\zeta\left(3\right)}\right)\frac{p^2dp}{e^{E(p)/T}+1}, \end{aligned} \quad (5.7)$$

where $E(p) = (p^2+m^2)^{1/2}$, and $E(p)\approx p$ in the relativistic kinematics limit. In this expression $\eta_{\nu_\alpha} = \mu_{\nu_\alpha}/T$ is the degeneracy parameter (chemical potential divided by temperature) for neutrino species ν_α and $F_2(\eta) \equiv \int_0^\infty x^2dx/(e^{x-\eta}+1)$ is the relativistic Fermi integral of order 2 [$F_2(0) = (3/2)\zeta(3)$]. The distribution function for a neutrino species α is

$$f_\alpha(p,t) = 1/(e^{E(p)/T-\eta_{\nu_\alpha}}+1). \quad (5.8)$$

The last approximation in Eq. (5.7) follows if we take the neutrino degeneracy parameter to be zero. This is frequently a good approximation for almost all of the range of lepton numbers which are interesting for our purposes. However, it may not be valid over the broader range of allowed lepton numbers given in Eqs. (4.2) and (4.3). For small lepton numbers $\eta_{\nu_\alpha}\approx 1.46L_{\nu_\alpha}$; in fact, whenever ν_α has relativistic kinematics, we can write

$$L_{\nu_\alpha} \approx \frac{1}{4\zeta(3)}\left\{\frac{\pi^2}{3}\eta_{\nu_\alpha} + \frac{1}{3}\eta_{\nu_\alpha}^3\right\}. \quad (5.9)$$

This equation can easily be inverted to find $\eta_{\nu_\alpha}(L_{\nu_\alpha})$.

In the early universe, for temperature ranges where the number of degrees of freedom is constant, the time-temperature relation is a simple power law and the quantity $\epsilon\equiv p/T$ is a comoving invariant. The differential number density for small lepton number in this case is then

$$dn_{\nu_\alpha} \approx \left(\frac{n_\gamma}{4\zeta\left(3\right)}\right)\frac{\epsilon^2 d\epsilon}{e^\epsilon+1}. \quad (5.10)$$

B. Quantitative formulation for the early universe

If one makes the assumption that the only net lepton number in the universe is that required for electric charge neutrality (*i.e.*, half of the baryon number when there are equal numbers of protons and neutrons), then the finite density potential usually remains negligible. In some cases where $\delta m^2<0$, an initially small asymmetry like this can be amplified by matter-enhanced active-sterile conversion [59, 60].

The finite density potential in the early universe could be dominated by asymmetries in the lepton number, and so is often referred to as the "lepton potential." It takes the form

$$V^D = \frac{2\sqrt{2}\zeta(3)}{\pi^2}G_{\rm F}T^3\left(\mathcal{L}^\alpha \pm \frac{\eta}{4}\right), \quad (5.11)$$

where we take "+" for $\alpha = e$ and "−" for $\alpha=\mu,\tau$. Here we define the net driving lepton number $\mathcal{L}^\alpha$ in terms of the lepton numbers in each active neutrino species as

$$\mathcal{L}^\alpha \equiv 2L_{\nu_\alpha} + \sum_{\beta\neq\alpha} L_{\nu_\beta} \quad (5.12)$$

with the final sum over the active neutrino flavors other than ν_α. Note that in Eq. (5.11), the baryon-to-photon ratio is η, not to be confused with neutrino degeneracy parameter.

The total weak potential, $V(p,T) = V^D(T)+V^T(p,T)$, experienced by an active neutrino ν_α is approximately

$$V\left(p,T\right) \approx (40.2\,{\rm eV})\left(\frac{\mathcal{L}}{10^{-2}}\right)\left(\frac{T}{\rm GeV}\right)^3 - Bp\left(\frac{T}{\rm GeV}\right)^4. \quad (5.13)$$

As noted above, the thermal potential V^T must take into account the presence of populated leptons of the same flavor. For ν_e this is required at all temperatures where the neutrinos are coupled; for ν_μ, the thermal muon term should be included at temperatures $T\gtrsim 20\,{\rm MeV}$, where the μ is populated; and for ν_τ, the thermal term should be included at $T\gtrsim 180\,{\rm MeV}$. Therefore, the coefficient B takes on the values:

$$B \approx \begin{cases} 10.79\,{\rm eV} & \alpha = e \\ 3.02\,{\rm eV} & \alpha=\mu,\tau \end{cases} \quad (5.14)$$

for $T\lesssim 20\,{\rm MeV}$;

$$B \approx \begin{cases} 10.79\,{\rm eV} & \alpha = e,\mu \\ 3.02\,{\rm eV} & \alpha=\tau \end{cases} \quad (5.15)$$

for $20\,{\rm MeV}\lesssim T\lesssim 180\,{\rm MeV}$;

$$B \approx 10.79\,{\rm eV} \quad \alpha = e,\mu,\tau \quad (5.16)$$

for $T\gtrsim 180\,{\rm MeV}$.

The trend of the weak potential experienced by an active neutrino species ν_α is clear. When the quantity $\mathcal{L}\pm\eta/4$ is sufficiently large and positive (negative for $\bar\nu_\alpha$) the potential will rise with increasing temperature, reach a maximum, and then turn over and eventually become negative at a high temperature where thermal

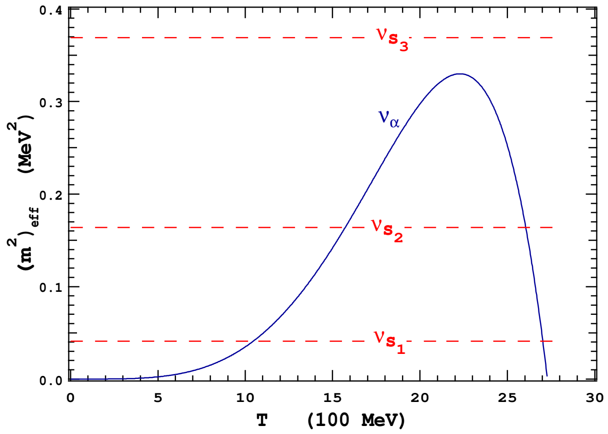

FIG. 1: An example of the temperature evolution of the active and sterile neutrino effective mass-squared, $m^2_{\rm eff}$. The active neutrino $m^2_{\rm eff}$ is dominated by a positive finite density potential at lower temperatures and turns over when the thermal potential dominates. Resonance occurs at level crossings, where the active and sterile $m^2_{\rm eff}$ tracks intersect.

terms dominate. The potential as a function of temperature for some representative parameters is shown as the solid line in Fig. 1. With this behavior it is obvious that neutrino mass level crossings in the temperature regime *not* dominated by the thermal terms are possible only if the vacuum mass eigenvalues most closely associated with some sterile neutrinos are larger than those most closely associated with ν_α.

VI. NON-EQUILIBRIUM PRODUCTION: THE STERILE NEUTRINO BOLTZMANN EQUATION

The Boltzmann equation gives the evolution of the phase-space density distribution function $f(p,t)$ for a particle species. For sterile neutrinos in the early universe, it can be written as [66, 67]

$$\frac{\partial}{\partial t} f_s(p,t) - H\,p\,\frac{\partial}{\partial p} f_s(p,t) = \sum_i \int \Gamma_i(p'_\alpha,p) f_\alpha(p'_\alpha,t)\,[1-f_s(p,t)]\,d^3p'_\alpha - \int \Gamma_i(p'_\alpha,p) f_s(p,t)\,[1-f_\alpha(p'_\alpha,t)]\,d^3p'_\alpha, \quad (6.1)$$

where the rate of scattering production of ν_s corresponding to a particular channel i [see Eq. (6.8)] is Γ_i. We make two approximations regarding the scattering kernels $\Gamma_i(p',p)$: (1) they are isotropic; and (2) they are conservative.

The first of these approximations is completely justified given a homogeneous and isotropic universe. The second—that an active neutrino scatters into a sterile state of the same energy—is made purely to ease the computational complexity of following the evolving system of neutrinos. We note, however, that Ref. [68] estimates the effects of relaxing this approximation in the context of a semi-analytic calculation and find that it makes little qualitative or quantitative difference in the results.

Certainly, however, a better treatment could be extended to the scattering kernel. This could, for example, change the conditions required for coherence. For example, we note that the effects described in Ref. [69] may be important, especially regarding where coherence breaks down. We show, however, in Sec. VII that coherent production of sterile neutrinos at MSW resonances is not important in our favored parameter regime.

In our discussion, we take $f_i(p,t)$ to be the momentum- and time-dependent distribution function of active ($\alpha = e,\mu,\tau$) and sterile (s) neutrinos. The distribution functions f_α are given by Eq. (5.8). The second left hand side term arises from the redshifting of the distribution.

However, Eq. (6.1) is semi-classical in its evolution of the neutrino distributions. To exactly follow the full quantum development, including such quantum effects as damping and off-diagonal contributions to the neutrino Hamiltonian in matter [70], one must follow the time evolution of the density matrix [71–74]. One can approximate the effects of quantum damping through a damped conversion rate $\Gamma(\nu_\alpha \to \nu_s; p, t)$. Fermi blocking effects are taken to be negligible, leaving the Boltzmann equation as

$$\frac{\partial}{\partial t} f_s(p,t) - H\,p\,\frac{\partial}{\partial p} f_s(p,t) \approx \Gamma(\nu_\alpha \to \nu_s; p,t)\,[f_\alpha(p,t) - f_s(p,t)]\,. \quad (6.2)$$

The reverse term is important for the $L \neq 0$ case, where f_α and f_s can become comparable for certain regions of the neutrino momentum distributions.

The conversion rate to sterile neutrinos is just the product of half of the *total* interaction rate, Γ_α, of the neutrinos with the plasma and the probability that an active neutrino has transformed to a sterile:

$$\Gamma(\nu_\alpha \to \nu_s; p,t) \approx \frac{\Gamma_\alpha}{2} \langle P_m(\nu_\alpha \to \nu_s; p,t)\rangle. \quad (6.3)$$

This probability P_m depends on the amplitude of the matter mixing angle and the quantum damping rate $D(p) = \Gamma_\alpha(p)/2$ [$\bar D(p) = \bar\Gamma_\alpha(p)/2$] for neutrinos [antineutrinos] [75–78],

$$\langle P_m(\nu_\alpha \to \nu_s; p, t)\rangle \approx \frac{1}{2}\frac{\Delta(p)^2\sin^2 2\theta}{\Delta(p)^2\sin^2 2\theta + D^2(p) + [\Delta(p)\cos 2\theta - V^D - V^T(p)]^2} \tag{6.4}$$

$$\langle P_m(\bar\nu_\alpha \to \bar\nu_s; p, t)\rangle \approx \frac{1}{2}\frac{\Delta(p)^2\sin^2 2\theta}{\Delta(p)^2\sin^2 2\theta + \bar D^2(p) + [\Delta(p)\cos 2\theta + V^D - V^T(p)]^2} \tag{6.5}$$

The full Boltzmann equation then is

$$\begin{aligned}
\frac{\partial}{\partial t} f_s(p,t) - H\,p\,\frac{\partial}{\partial p} f_s(p,t) &\approx \frac{\Gamma_\alpha(p)}{2}\langle P_m(\nu_\alpha \to \nu_s, t_{\rm in} + \tau)\rangle_\tau\,[f_\alpha(p,t) - f_s(p,t)] \\
&\approx \frac{\Gamma_\alpha(p)}{2}\sin^2 2\theta_m\left[1 + \left(\frac{\Gamma_\alpha(p) l_m}{2}\right)^2\right]^{-1}[f_\alpha(p,t) - f_s(p,t)] \\
&\approx \frac{1}{4}\frac{\Gamma_\alpha(p)\Delta^2(p)\sin^2 2\theta}{\Delta^2(p)\sin^2 2\theta + D^2(p) + [\Delta(p)\cos 2\theta - V^L - V^T(p)]^2}\,[f_\alpha(p,t) - f_s(p,t)]\,,
\end{aligned} \tag{6.6}$$

where $\{1+[\Gamma_\alpha(p)l_m/2]^2\}^{-1}$ is the damping factor. There are analogous equations for Eqs. (6.1)-(6.3) and Eq. (6.6) for antineutrinos.

Previous calculations have approached the solution of this equation for the case of negligible lepton number ($L \approx 0$) analytically and have been restricted to the short epoch just prior to BBN where the Hubble expansion rate H (evolution of the scale factor) and time-temperature relations are simple power laws (the temperature is proportional to the inverse scale factor) [10, 68]. Such approximations allow the reduction of the left-hand side of Eq. (6.6) to a single term. With the approximations that lepton number $\mathcal{L}$ is always negligible, that the thermal term V^T is not modified by population of leptons, that the interaction rate is not enhanced due to population of scatterers, that quantum damping is never important, and that the reverse rates ($\nu_s \to \nu_\alpha$) are always negligible, then the right hand side can also be considerably simplified, and the solution for the sterile neutrino dark matter abundance is reduced to a simple integral. It is obvious, however, that many if not all of these approximations are eventually invalid over at least some of the parameter range of interest for sterile neutrino dark matter.

For example, in order to probe cases where sterile neutrino dark matter production may lie above the QCD transition ($T \gtrsim 100\,\mathrm{MeV}$), and in order to improve the accuracy of the predicted dark matter contribution, we must extend our calculation to epochs where the scale factor-temperature and time-temperature relations are not simple power laws (see the Appendix for details). The interactions contributing to $\Gamma_\alpha(p)$ which produce (and remove) sterile neutrinos are

$$\begin{aligned}
\nu_\alpha + \nu_\beta &\rightleftharpoons \nu_\alpha + \nu_\beta \\
\nu_\alpha + l^\pm &\rightleftharpoons \nu_\alpha + l^\pm \\
\nu_\alpha + q &\rightleftharpoons \nu_\alpha + q \\
\nu_\alpha + \nu_\alpha &\to l^+ + l^-.
\end{aligned} \tag{6.7}$$

Here, the ν_α represent either neutrinos or anti-neutrinos, as appropriate, and q and l are any populated quark and charged lepton flavors. The total interaction rate at temperatures $1\,\mathrm{MeV} \lesssim T \lesssim 20\,\mathrm{MeV}$ due to interactions of the neutrinos among themselves and the $e^\pm$ pairs is

$$\Gamma_\alpha(p) \approx \begin{cases} 1.27\,G_{\rm F}^2 p T^4, & \alpha = e, \\ 0.92\,G_{\rm F}^2 p T^4, & \alpha = \mu, \tau. \end{cases} \tag{6.8}$$

At higher temperatures, other leptons and quarks are populated and contribute to the neutrino interaction rate. In our calculations, we have included the enhancement of the interaction rate due to the presence of these new particles in the plasma at high temperatures. In particular, a significant increase to the scattering rate results at temperatures above the QCD scale. Interestingly, the results of the production of sterile neutrino dark matter therefore depend on the temperature of the QCD transition, where the quark-antiquark pairs annihilate and are incorporated into color singlets.

The high scattering rate characteristic of the environment of the early universe not only serves to populate the sterile neutrino sea, but can also suppress the production of sterile neutrinos when the matter oscillation length is large compared to the mean free path of the neutrinos. When the oscillation length is much larger than the mean free path, the probability that an active neutrino has transformed into a sterile state becomes very small. It can be shown that such scattering can force a quantum system to not evolve from the initial state [75, 79]. Essentially, each scattering event resets the phase of the developing neutrino state $|\Psi_{\nu_\alpha}\rangle$. This is the so-called quantum Zeno effect.

Consider the right hand side collision term in Eq. (6.2). The sterile neutrinos are initially not in thermal equilibrium, and therefore the reverse processes are initially unimportant. They will, however, become more important as the sterile neutrino sea is populated. Because the sterile neutrinos are *never* in equilibrium, the usual simplifying principle of steady-state equilibrium [67, 80] cannot be made. Therefore, to calculate the production of sterile species, we must start with the Boltzmann equation in its "unintegrated" form Eq. (6.6).

We have directly solved the Boltzmann equation numerically for the $L \approx 0$ case (*e.g.*, $L \approx 10^{-10}$), and found the amount of sterile neutrino dark matter produced for a broad range of sterile neutrino mass and mixing angles with each of the three active neutrino flavors. In treating the redshift of the sterile distribution, we have greatly accelerated the numerical calculation by following the redshift of the sterile neutrino distribution function f_s by redshifting momenta as $p \propto t^{-1/2}$, which is always true in a radiation dominated universe (a necessary condition for BBN and the CMB). This numerical method allows us to correctly follow the redshifting of the sterile neutrino without the second term of the Liouville operator in the Boltzmann equation (6.6), while active neutrinos may be reheated via annihilation of other species.

The contribution to the closure fraction of the universe, meeting all constraints (see Secs. IX and X) is shown in Fig. 2 for $\nu_e \rightleftharpoons \nu_s$ and Fig. 3 for $\nu_\tau \rightleftharpoons \nu_s$. A general fit to our results for nonresonant production is

$$\Omega_{\nu_s} h^2 \approx 0.3 \left(\frac{\sin^2 2\theta}{10^{-10}}\right)\left(\frac{m_s}{100\,\mathrm{keV}}\right)^2. \qquad (6.9)$$

The maximum rate of sterile neutrino production occurs at temperature [10, 81]

$$T_{\max} \approx 133\,\mathrm{MeV}\left(\frac{m_s}{1\,\mathrm{keV}}\right)^{1/3}. \qquad (6.10)$$

The closure fraction contribution for $\nu_\mu \rightleftharpoons \nu_s$ is nearly identical to $\nu_\tau \rightleftharpoons \nu_s$. The particular flavor(s) of the active neutrino with which the sterile neutrino mixes does determine to some extent the ultimate closure fraction. However, this flavor dependence is negligible for larger ν_s masses since, from Eq. (6.10), for sterile neutrinos with $m_s \gtrsim 2\,\mathrm{keV}$, $T_{\max} \gtrsim 180\,\mathrm{MeV}$. At these temperatures, $e^\pm$, $\mu^\pm$ and even $\tau^\pm$ (due to the high entropy of the universe) are populated significantly, so that the thermal potentials are identical for all flavors. Therefore, the mass fractions produced for all flavors with sterile neutrino masses $m_s \gtrsim 2\,\mathrm{keV}$ are very similar.

The similarity of the results of production for ν_e, ν_μ, and ν_τ mixing with a sterile neutrino is at odds with the calculation of Ref. [68]. There are several differences between our treatment and that of Ref. [68] that can account for the disparity in results. First, the primary cause for discrepancy for the $\nu_\tau \rightleftharpoons \nu_s$ neutrino mixing case is likely to lie in the fact that τ leptons are significantly populated at temperatures one-tenth of their mass ($T \gtrsim 177\,\mathrm{MeV}$) due to the high-entropy of the universe. This modifies the thermal term in Eq. (5.6) in an important way, not included in Ref. [68]. In our work, we follow the number and energy density of tau leptons explicitly in our numerical evolution. One can see from Eq. (6.10) that for masses of sterile neutrinos greater than about 2 keV, production occurs at a temperature where the τ lepton is significantly populated. Second, the population of massive species of scatterers (μ and τ leptons and u, d, s, c, b quarks) which enhance the scattering rate is not included in Ref. [68], but are included in our calculations. Third, effects of re-heating on the dilution of sterile neutrino dark matter are treated only approximately in Ref. [68]. We explicitly include reheating and dilution in our calculation through our treatment of the time-temperature evolution of active and sterile neutrinos, as described in the Appendix.

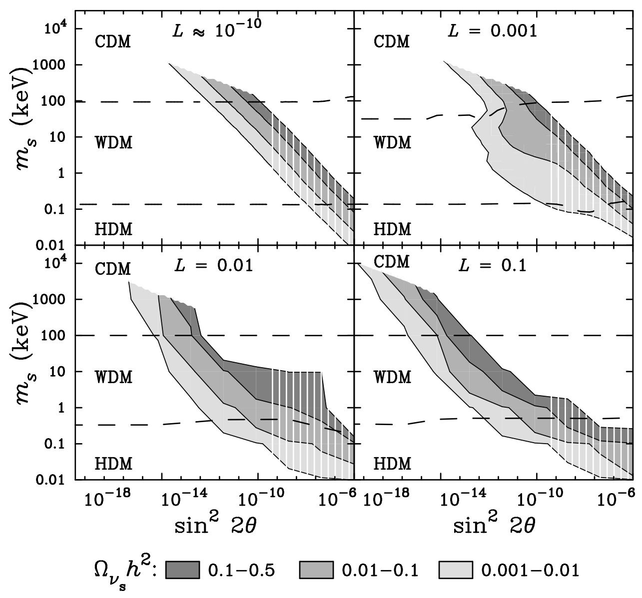

FIG. 2: Regions of $\Omega_{\nu_s} h^2$ produced by resonant and nonresonant $\nu_e \leftrightarrow \nu_s$ neutrino conversions for selected net lepton number L, after applying all constraints (see Secs. IX and X). Regions of parameter space disfavored by supernova core collapse considerations are shown with vertical stripes.

VII. INITIAL LEPTON NUMBER AND RESONANT PRODUCTION

In this section, we examine the resonant production of sterile neutrino dark matter for a range of initial lepton numbers. We will extend the treatment of this issue given in Shi and Fuller [11] considering the effects of particle annihilation and reheating and enhanced scattering rates on coherent and incoherent evolution through MSW resonances. This allows us to consider resonant $\nu_\alpha \rightleftharpoons \nu_s$ conversion at high temperature epochs in the early universe, up to the electroweak transition regime at $T \approx 100\,\mathrm{GeV}$.

Resonance, or mass level crossings as seen in Fig. 1, are characterized by maximal effective matter mixing angles $(\theta_m)_{\mathrm{res}} = \pi/4$, where the $\nu_\alpha \to \nu_s$ conversion rate is,

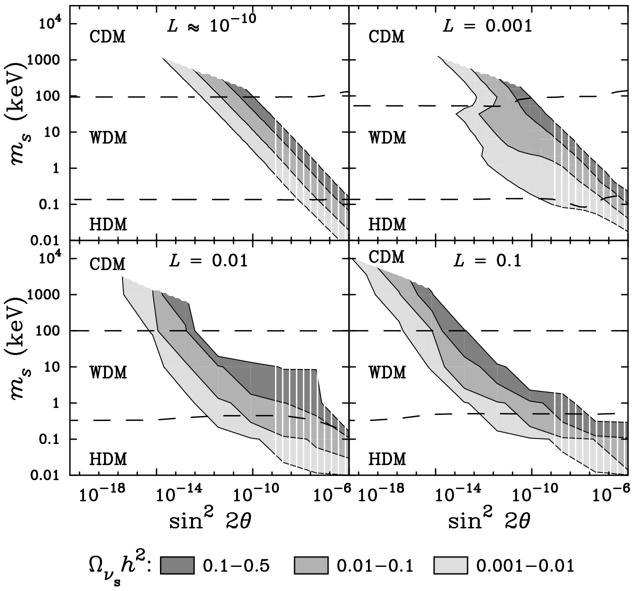

FIG. 3: Same as Fig. 2, but for $\nu_\tau \leftrightarrow \nu_s$.

consequently, enhanced. The resonance condition is

$$\Delta(p)\cos 2\theta - V^L - V^T(p) = 0$$

$$\Delta(p)\cos 2\theta - (40.2\,\text{eV})\left\{\frac{\mathcal{L}\pm\eta/4}{10^{-2}}\right\}\left(\frac{T}{\text{GeV}}\right)^3 + B\epsilon\left(\frac{T}{\text{GeV}}\right)^5 = 0$$

$$\left(\frac{m_s}{1\,\text{keV}}\right)^2\cos 2\theta \approx 8.03\ \epsilon\left\{\frac{\mathcal{L}\pm\eta/4}{10^{-2}}\right\}\left(\frac{T}{100\,\text{MeV}}\right)^4 + 2\epsilon^2\left(\frac{B}{\text{keV}}\right)\left(\frac{T}{100\,\text{MeV}}\right)^6. \qquad (7.1)$$

Choose one of the horizontal dotted lines laying below the peak of the solid line in Fig. 1. This indicates the "mass track" for a sterile neutrino species. This is, of course, simply the vacuum mass-squared value $(m^2_{\text{eff}})_s = m_s^2$, and is flat and independent of temperature. The effective mass-squared track for an active neutrino ν_α could be as shown in Fig. 1. Mass level crossings (resonances) in the $\nu_\alpha \rightleftharpoons \nu_s$ system can occur when m_s^2 lies below the peak value of $(m^2_{\text{eff}})_{\nu_\alpha}$. This peak will occur at temperature

$$T_{\text{PEAK}} \approx \left(\frac{2}{3}\right)^{1/2} T_0 \approx \left(\frac{4\sqrt{2}\zeta(3)}{3\pi^2}\right)^{1/2}\epsilon^{-1/2}\{\mathcal{L}\pm\eta/4\}^{1/2} \times\left[\frac{G_F(\text{GeV})^5}{B}\right]^{1/2} \approx (2.98\,\text{GeV})\epsilon^{-1/2}\left(\frac{\mathcal{L}}{10^{-2}}\right)^{1/2}, \qquad (7.2)$$

where T_0 is the high temperature at which the effective mass-squared track crosses zero, and where in the last numerical expression we have assumed that $T > 180\,\text{MeV}$.

Note that the peak value of effective mass-squared, or equivalently, the largest value of $\delta m^2 \cos 2\theta$ for which a level crossing can occur is,

$$m^2_{\text{eff}}(T_{\text{PEAK}}) = \left(\delta m^2\cos 2\theta\right)_{m^2_{\text{eff(PEAK)}}} \approx \left(\frac{4\sqrt{2}\zeta(3)}{3\pi^2}\right)^3\frac{\{\mathcal{L}\pm\eta/4\}^3}{\epsilon}\left[\frac{G_F^3(\text{GeV})^{10}}{B^2}\right]. \qquad (7.3)$$

For example, we can show that the largest ν_s mass which can have a resonance with a ν_e is roughly

$$(m_s)_{\text{PEAK}} \approx \frac{406\,\text{keV}}{\epsilon^{1/2}}\left(\frac{\mathcal{L}}{10^{-2}}\right)^{3/2}. \qquad (7.4)$$

As the universe expands, an active neutrino species ν_α will encounter two resonances with a sterile neutrino species, as long as this sterile species has m_s^2 less than the peak value of m^2_{eff} in Eq. (7.3). At some epochs, both resonances may be present in a given active neutrino spectrum since the resonance condition, Eq. (7.1), has more than one zero. This behavior is shown for a particular case in Fig. 4.

What is the effect of resonance on sterile neutrino production in the early universe? The answer to this question depends on the rate of incoherent production at the resonance, whether the neutrinos are coherent as they pass through resonance and, if they are coherent, the degree of adiabaticity characterizing the evolution of the neutrino flavor amplitudes through the resonance. There are two processes by which resonance affects neutrino conversion in the early universe: (1) enhanced incoherent conversion of those neutrinos at the resonance and (2) coherent MSW transformation of neutrinos passing through the resonance. The rate of incoherent production can be calculated numerically through the semi-classical Boltzmann evolution, Eq. (6.6).

The statistical formulation of both coherent and incoherent production can be described by the time evolution of the density matrix for the two neutrino states [70–75]. We show below that the masses and mixing angles of interest for sterile neutrino dark matter considered

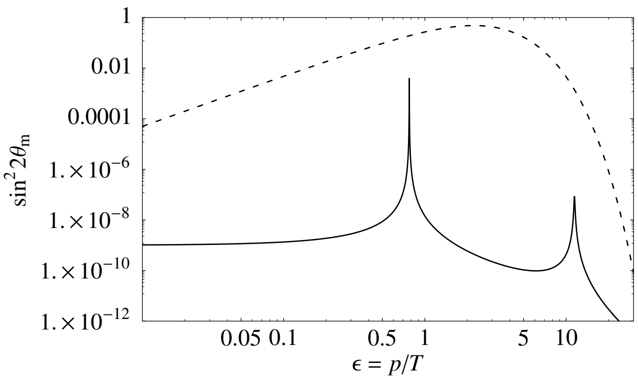

FIG. 4: The effective matter mixing $\sin^2 2\theta_m$ is shown for a case with two resonances (solid line). For this case, $m_s = 1\,\mathrm{keV}$, $\sin^2 2\theta = 10^{-9}$, $L = 6\times 10^{-4}$, and $T = 130\,\mathrm{MeV}$. The dashed line is the active neutrino energy distribution.

here give coherence across the relevant resonance width, but usually imply that the neutrino amplitude evolution through resonance is nonadiabatic. (Adiabatic evolution at lower mixing angle could occur at epochs where the entropy is being transferred from annihilating particles and where, as a consequence, the temperature and density do not change rapidly or are constant with time, *e.g.*, the QCD transition [82].)

Though the expansion rate of the universe scales as T^2, the active neutrino scattering rate scales as $G_F^2 T^5$. For neutrino flavor evolution through resonances, the coherence condition will be met only when the inverse of the scattering rate (the active neutrino mean free path) is much larger than the resonance width or

$$\begin{aligned} T &\ll \left(\frac{4\pi^3}{5}\right)^{1/6} \frac{g^{1/6}}{m_{\rm pl}^{1/3} G_F^{2/3} \tan^{1/3} 2\theta} \\ &\approx 140\,\mathrm{MeV}\frac{(g/100)^{1/6}}{\left(\sin^2 2\theta/10^{-10}\right)^{1/6}}. \end{aligned} \quad (7.5)$$

(Here, $m_{\rm pl} \approx 1.22\times 10^{22}\,\mathrm{MeV}$ is the Planck mass.) Therefore, for the mixing angles relevant here ($\sin^2 2\theta \lesssim 10^{-10}$), at temperatures below 140 MeV, the resonance could in principle drive coherent $\nu_\alpha \rightleftharpoons \nu_s$ transformation. The efficiency of MSW conversion relies on the adiabaticity of the evolution through the resonance region.

The width of the resonance is the product of the local density scale height of weak charges and $\tan 2\theta$. In turn, the biggest share of the density scale height is determined by the expansion rate of the universe, $H \approx (8\pi^3/90)^{1/2} g^{1/2} T^2/m_{\rm pl}$, where the statistical weight in relativistic particles, g, has contributions from both bosons g_b and fermions g_f:

$$g = \sum_i (g_b)_i + 7/8 \sum_i (g_f)_i. \quad (7.6)$$

In fact, once neutrino flavor transformation begins, the inherent nonlinearity of this process can have a sizable, even dominant effect on the density scale height. Ignoring this, the resonance width expressed in time is $\delta t \approx (2/3)t(\tan 2\theta) = (1/3)H^{-1}\tan 2\theta$, where $t \approx (1/2)H^{-1}$ is the age of the universe at an epoch with temperature T in radiation dominated conditions. [The particle horizon is H^{-1}, so that, absent large scale neutrino flavor transformation, the resonance width is a constant fraction $(1/3)\tan 2\theta$ of the horizon scale.]

The effective matter mixing angle for the oscillation channel $\nu_\alpha \rightleftharpoons \nu_s$ at an epoch with temperature T is

$$\sin^2 2\theta_m = \left\{1 + \frac{\left[1 - 2\epsilon T V/\left(\delta m^2 \cos 2\theta\right)\right]^2}{\tan^2 2\theta}\right\}^{-1}. \quad (7.7)$$

At resonance, $\sin^2 2\theta_m = 1$, so that one resonance width off resonance this effective mixing will have fallen to $\sin^2 2\theta_m = 1/2$. Clearly, the change in effective weak potential over this interval is $\delta V \approx \delta m^2 \sin 2\theta/(2\epsilon T_{\rm res})$, where $T_{\rm res}$ is the resonance temperature for neutrino spectral parameter ϵ. From this it can be seen that $(\delta V/V)_{\rm res} = \tan 2\theta$ and it follows that the resonance width is

$$\delta t = \frac{\delta t}{\delta V}\delta V \approx \left|\frac{1}{V}\cdot\frac{dV}{dt}\right|_{\rm res}^{-1} \tan 2\theta. \quad (7.8)$$

The neutrino oscillation length at resonance is $l_m^{\rm res} = (4\pi\epsilon T_{\rm res})/(\delta m^2 \sin 2\theta) = 2\pi/\delta V$, and the adiabaticity parameter is proportional to the ratio $\delta t/l_m^{\rm res}$, and is defined as

$$\gamma \equiv 2\pi\frac{\delta t}{l_m^{\rm res}} \approx (\delta V)^2 \left|\frac{d\epsilon}{dV}\Big/\frac{d\epsilon}{dt}\right|_{\rm res}. \quad (7.9)$$

When there are many oscillation lengths within the resonance width (*i.e.*, when $\gamma \gg 1$) neutrino flavor evolution will be adiabatic and we can then expect efficient flavor conversion at resonance. [Given the small vacuum mixing angles relevant for this work and consequent small widths, the Landau-Zener jump probability [83] with the form $P_{\rm LZ} \approx \exp(-\pi\gamma/2)$ gives an adequate gauge of the probability of $\nu_\alpha \to \nu_s$ conversion at resonance, $1 - P_{\rm LZ}$.]

The physical interpretation of Eq. (7.9) is straightforward. The adiabaticity parameter is proportional to the energy width of the resonance divided by the "sweep rate," $d\epsilon/dt$, of the resonance energy through the neutrino distribution function. The resonance sweep rate is determined mostly by the expansion rate of the universe (an inverse gravitational time scale), but the rate of change of lepton number $\mathcal{L}$ as $\nu_\alpha \to \nu_s$ proceeds can become important, even paramount as lepton number is used up and $\mathcal{L} \to 0$.

The resonance energy width scaled by temperature is $\delta\epsilon \approx \delta V \left|d\epsilon/dV\right|_{\rm res} \approx \epsilon_{\rm res}\tan 2\theta$, where $\epsilon_{\rm res}$ is the resonant value of the neutrino spectral parameter at $T_{\rm res}$. If we confine our discussion to resonances on the low temperature side of $T_{\rm PEAK}$, where the thermal terms in the potential can be neglected, then

$$\epsilon_{\rm res} \approx \frac{\delta m^2 \cos 2\theta}{(4\sqrt{2}\zeta(3)/\pi^2) G_{\rm F} T^4 \mathcal{L}} \tag{7.10}$$
$$\approx 0.1245 \left(\frac{\delta m^2 \cos 2\theta}{1\,{\rm keV}^2}\right)\left(\frac{10^{-2}}{\mathcal{L}}\right)\left(\frac{100\,{\rm MeV}}{T}\right)^4.$$

As the universe expands and cools with time, and for a given δm^2, the resonance will sweep through the ν_α energy distribution function from low to high neutrino spectral parameter ϵ. In this same limit of resonance below $T_{\rm PEAK}$, the sweep rate is

$$\frac{d\epsilon}{dt} \approx 4\epsilon H \left(1 - \frac{\dot{\mathcal{L}}}{4H\mathcal{L}}\right), \tag{7.11}$$

where $\dot{\mathcal{L}}$ is the time rate of change of the lepton number resulting from neutrino flavor conversion. Since the expansion rate scales as $H \sim T^2$, the prospects for adiabaticity are better at lower temperatures and later epochs in the early universe, all other parameters being the same.

From Eqs. (7.9), (7.10), and (7.11), we can estimate that at resonance the degree of adiabaticity is

$$\gamma \approx \frac{\delta m^2}{2\epsilon T_{\rm res}} \frac{\sin^2 2\theta}{\cos 2\theta} \left(4\frac{\dot{T}}{T} + \frac{\dot{\mathcal{L}}}{\mathcal{L}}\right)^{-1} \tag{7.12}$$
$$\approx \frac{3\sqrt{5}\zeta(3)^{3/4}}{2^{17/8}\pi^3} \frac{(\delta m^2)^{1/4}\, m_{\rm pl}\, G_{\rm F}^{3/4} \mathcal{L}^{3/4}}{g^{1/2}\epsilon^{1/4}\left|1 - \dot{\mathcal{L}}/4H\mathcal{L}\right|} \frac{\sin^2 2\theta}{\cos^{7/4} 2\theta}$$
$$\approx \left(\frac{m_s}{1\,{\rm keV}}\right)^{1/2} \left(\frac{10.75}{g}\right)^{1/2} \left(\frac{\mathcal{L}}{10^{-2}}\right)^{3/4} \frac{1}{\left|1 - \dot{\mathcal{L}}/4H\mathcal{L}\right|}$$
$$\times \left(\frac{1}{\epsilon_{\rm res}}\right)^{1/4} \left\{\frac{\sin^2 2\theta}{7.5\times 10^{-10}}\right\}, \tag{7.13}$$

where in the second equality we assume the standard radiation-dominated conditions and expansion rate, and where in the final equality we have employed the approximation $\delta m^2 \approx m_s^2$, valid when $m_s \gg m_{\nu_\alpha}$, and where we have assumed that the vacuum mixing angle is small. Here we see that for the mixing angles allowed by our constraints, $\sin^2 2\theta < 10^{-9} (3\times 10^{-10})$ for $\nu_\mu, \nu_\tau (\nu_e)$ mixing with sterile neutrinos, and masses $m_s \gtrsim 1\,{\rm keV}$, the resonance is not adiabatic.

We conclude that the main effect of resonance is enhancement of scattering-induced incoherent conversion of neutrinos with energies in the resonant region. Therefore, the formulation of the semi-classical Boltzmann Equation (6.6) is appropriate for calculating the total production of sterile neutrinos in the early universe.

The results of our numerical calculations can be seen in Fig. 2 for $\nu_e \rightleftharpoons \nu_s$ and in Fig. 3 for $\nu_\tau \rightleftharpoons \nu_s$ for the cases where initially $L = 0.001, 0.01, 0.1$. The calculation includes both nonresonant scattering production and matter-enhanced (resonant) production. Examples of the resulting sterile neutrino energy spectra are shown in Fig. 5. Resonantly produced sterile neutrinos tend to have energy spectra appreciably populated only at the low ϵ end. This results from the resonant energy starting at the lowest momenta and moving through higher momenta neutrinos [see Eq. (7.10)] as the universe cools and lepton number is depleted through conversion into a sterile neutrino population.

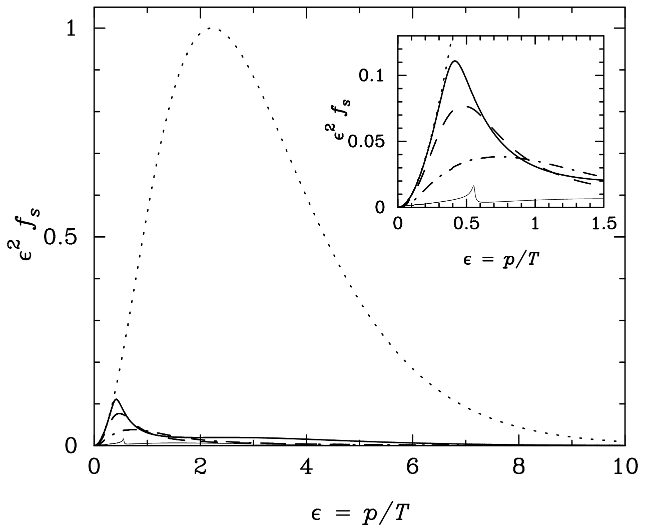

FIG. 5: The sterile neutrino distribution for four cases of resonant and non-resonant $\nu_e \leftrightarrow \nu_s$, as described in the text. The dotted line is a normalized active neutrino spectrum. The thick-solid, dashed, dot-dashed, and thin-solid lines correspond to cases (1)–(4), respectively. The inset shows a magnified view of the low momenta range of the distributions.

Figure 5 shows the resulting spectrum for four sample cases of sterile neutrino dark matter production:

(1) $m_s = 0.8$ keV, $\sin^2 2\theta = 10^{-6}$, $L_{\rm init} = 0.01$, resulting in $\Omega_{\nu_s} h^2 = 0.25$ and $\langle p/T\rangle = 2.9$;

(2) $m_s = 1$ keV, $\sin^2 2\theta = 10^{-7}$, $L_{\rm init} = 0.01$, resulting in $\Omega_{\nu_s} h^2 = 0.13$ and $\langle p/T\rangle = 1.8$;

(3) $m_s = 1$ keV, $\sin^2 2\theta = 10^{-8}$, $L_{\rm init} = 0.01$, resulting in $\Omega_{\nu_s} h^2 = 0.10$ and $\langle p/T\rangle = 2.0$;

(4) $m_s = 10$ keV, $\sin^2 2\theta = 10^{-8}$, $L_{\rm init} = 0.001$, resulting in $\Omega_{\nu_s} h^2 = 0.57$ and $\langle p/T\rangle = 2.3$.

A particularly interesting case is (4), where the resonance passes through the distribution during the QCD transition, where the disappearance of degrees of freedom heats the photon and neutrino plasma, forcing the universe to cool more slowly. For this period, the resonance moves much more slowly through the spectrum and is consequently more efficient in $\nu_\alpha \to \nu_s$ conversion through that region of the neutrino energy spectra. This produces a "spike" in the sterile neutrino distribution (see Ref. [82]).

VIII. COLLISIONLESS DAMPING SCALE: HOT, WARM OR COLD NEUTRINOS

Given the sterile neutrino energy spectrum and number density, the transfer function for dark matter models can be calculated. Here, we instead give a rough guide based on the free streaming length at matter-radiation equality, λ_{FS}. Structures smaller than λ_{FS} are damped. This is because at early epochs where sterile or active neutrino species are relativistic, they can freely flow out of the regions of sizes smaller than λ_{FS} (very roughly the horizon size at the epoch where the neutrinos revert to nonrelativistic kinematics). Previous numerical work has shown that the free streaming scale is approximately [67, 84]

$$\lambda_{FS} \approx 40\,\mathrm{Mpc}\left(\frac{30\,\mathrm{eV}}{m_\nu}\right)\left(\frac{\langle p/T\rangle}{3.15}\right). \quad (8.1)$$

The mass contained within the free streaming length is then

$$M_{FS} \approx 2.6\times10^{11}\,M_\odot\ (\Omega_m h^2)\left(\frac{1\,\mathrm{keV}}{m_\nu}\right)^3\left(\frac{\langle p/T\rangle}{3.15}\right)^3, \quad (8.2)$$

where Ω_m is the contribution of all "matter" to closure. These values can give a guide as to the collisionless damping scale of sterile neutrino dark matter. In Fig. 6, we show contours of M_{FS} for the $\nu_\tau \rightleftharpoons \nu_s$ sterile neutrino production channel with $L = 0.01$. In Fig. 6, we assume that the universe is critically closed ($\Omega_m = 1$). Therefore, the contours are consistent with sterile neutrinos being the major constituent of dark matter near the dark gray regions where $\Omega_{\nu_s}h^2 = 0.1-0.5$.

In Figs. 2 and 3, we label the parameter regions corresponding to $M_{FS} > 10^{14}M_\odot$, $10^5M_\odot < M_{FS} < 10^{14}M_\odot$, and $M_{FS} < 10^5 M_\odot$ as HDM, WDM, and CDM, respectively. These definitions are somewhat arbitrary and here serve only as guides. Note that sterile neutrino mass by itself does not completely determine the free streaming (or collisionless damping) scale, since the inherent ν_s energy spectrum at production also helps to determine the ν_s kinematics at a given epoch. This latter effect is especially pronounced for nonthermal energy spectra, and is responsible, *e.g.*, for the non-flat collisionless damping mass scale lines in Fig. 6.

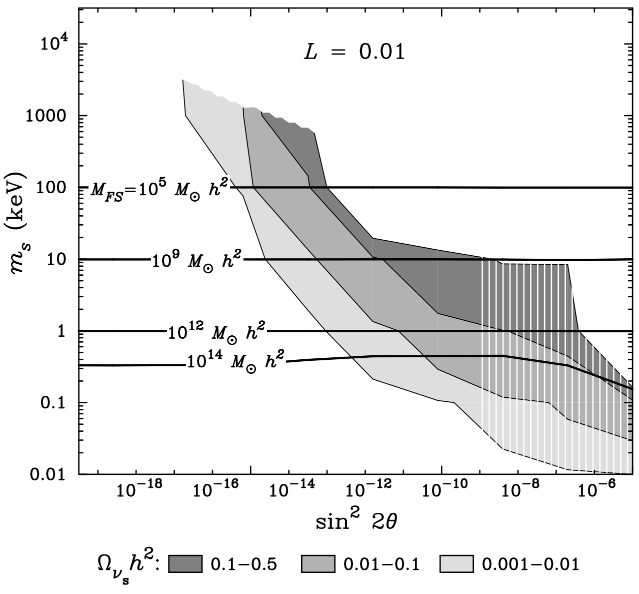

FIG. 6: The mass within the sterile neutrino free streaming length at matter-radiation equality (M_{FS}) in the $\nu_\tau \leftrightarrow \nu_s$, $L = 0.01$ case. Regions of parameter space disfavored by supernova core collapse considerations are shown with vertical stripes.

IX. COSMOLOGICAL CONSTRAINTS ON STERILE NEUTRINOS

A. Diffuse extragalactic background radiation

The decay rate of a massive sterile neutrino with vacuum mixing angle θ into lighter active neutrinos is [85]

$$\begin{aligned}\Gamma_{\nu_s} &\approx \sin^2 2\theta\, G_\mathrm{F}^2\left(\frac{m_s^5}{768\pi^3}\right) \quad (9.1)\\ &\approx 8.7\times10^{-31}\,\mathrm{s}^{-1}\left(\frac{\sin^2 2\theta}{10^{-10}}\right)\left(\frac{m_s}{1\,\mathrm{keV}}\right)^5.\end{aligned}$$

We have also included in our calculations the contributions to Γ_{ν_s} from visible and hadronic decays estimated from the partial decay widths of the Z^0 boson [7]. The rate of the corresponding radiative decay branch is smaller by a factor of $27\alpha/8\pi$ [86]:

$$\begin{aligned}\Gamma_{\nu_s\gamma} &\approx \sin^2 2\theta\ \alpha\ G_\mathrm{F}^2\left(\frac{9m_s^5}{2048\pi^4}\right) \quad (9.2)\\ &\approx 6.8\times10^{-33}\,\mathrm{s}^{-1}\left(\frac{\sin^2 2\theta}{10^{-10}}\right)\left(\frac{m_s}{1\,\mathrm{keV}}\right)^5.\end{aligned}$$

That these sterile neutrinos can decay stems from the fact that they are not truly "sterile," but have an effective interaction strength $\sim \sin^2_m 2\theta\ G_\mathrm{F}^2 = \sin^2 2\theta\ G_\mathrm{F}^2$, where the last equality is valid in vacuum (*i.e.*, at late epochs in the universe). Obviously, if a particle is going to be a dark matter candidate, it must have a lifetime τ at least of order the age of the universe ($t_\mathrm{today} \gtrsim 10\,\mathrm{Gyr}$). Regions of m_s vs $\sin^2 2\theta$ parameter space where $\tau < t_\mathrm{today}$ and not otherwise constrained are so labeled in Figs. 7 and 8. These parameters, corresponding to generally high sterile neutrino masses, guarantee that these particles decay away into lighter particles long before they clump in gravitational potential wells.

The radiative decay channel for sterile neutrinos can provide a constraint or a possible detection mode for some regions of the $m_s - \sin^2 2\theta$ parameter space. In particular, radiative decays of sterile neutrinos occuring between CMB decoupling and today could produce an appreciable flux of photons with energies comparable to m_s. In fact, there are firm upper limits on the flux from a diffuse photon component. For example, the total differential energy flux per unit solid angle for a DEBRA component is [27, 67, 87]

$$d\mathcal{F}/d\Omega \lesssim (1\,\mathrm{MeV}/E)\ \mathrm{cm}^{-2}\mathrm{sr}^{-1}\mathrm{s}^{-1}. \qquad (9.3)$$

As technology has progressed this limit on the true diffuse background has come down as distinct x-ray sources are resolved and their fluxes are removed from the count [88, 89]. At present the Chandra X-ray Observatory threatens to resolve a considerable fraction of the observed x-ray background (in the $0.5-8\,\mathrm{keV}$ band) into point and extended sources, primarily active galaxies, QSO's, and clusters.

Clearly, sterile neutrinos with radiative decay rates greater than an inverse Hubble time ($H^{-1} \approx 3.09 \times 10^{17}\,h^{-1}\,\mathrm{s} \approx 9.78\,h^{-1}\,\mathrm{Gyr}$) will tend to contribute background photons before the sterile neutrinos fall into potential wells and form structure. These photons will then produce a DEBRA contribution which must not exceed the overall limit in Eq. (9.3). Parameter regions violating this bound are labeled DEBRA in Figs. 7 and 8.

What about sterile neutrinos with much smaller radiative widths? These steriles could be decaying at more recent epochs, even today. However, if these are the dark matter (CDM or WDM), then they are not diffuse, but are strongly clustered. In Figs. 7 and 8 the regions with widely spaced vertical lines correspond to sterile neutrino mass and mixing properties that would give a DEBRA component in excess of the limit (9.3), *if* these steriles were distributed diffusely. Since most of the decay photons will be produced when the dark matter is in structure rather than diffuse, this region does not as yet constitute a constraint. Rather, it serves to define parameters that could give interesting x-ray fluxes in the gravitational potential wells of clusters of galaxies or other structures, depending on redshift, the cosmological parameters, and transfer functions and collisionless damping scales of the sterile neutrinos. Improved observations and models could lead to these regions turning into true constraints and may result in more stringent constraints or even lead to detection [90].

As an example, consider a large cluster of galaxies with dark matter mass $M \approx 10^{15}\,M_\odot$. The sterile neutrino decay luminosity in photons is

$$L \approx 7 \times 10^{36}\,\mathrm{erg\,s^{-1}} \left(\frac{\sin^2 2\theta}{10^{-10}}\right)\left(\frac{m_s}{1\,\mathrm{keV}}\right)^5. \qquad (9.4)$$

The observed x-ray luminosity for such clusters in the $1-10\,\mathrm{keV}$ band is $L_{\mathrm{cluster}} \sim 10^{45}\,\mathrm{erg\,s^{-1}}$ [91]. Clearly, for sterile neutrinos in our dark matter parameter space with masses of $20-30\,\mathrm{keV}$ and $\sin^2 2\theta \approx 10^{-11}$, the predicted luminosities may be comparable to those observed. The energy spectra may be different, however, and this could be an avenue for constraint.

B. Cosmic microwave background

Another constraint stems from the increase in energy density in relativistic particles due to massive sterile neutrino decay prior to cosmic microwave background (CMB) decoupling [92]. The BOOMERanG/MAXIMA observations [93] currently limit the effective number of neutrinos (N_ν) at decoupling to $N_\nu(\mathrm{CMB}) < 13$ at the 95% confidence level [55]. Measurements to higher multipole moments by the MAP and Planck probes will be able to further limit the relativistic energy present at decoupling. MAP may constrain $N_\nu(\mathrm{CMB}) < 3.9$, and the Planck mission could reach a limit $N_\nu(\mathrm{CMB}) < 3.05$ [94]. The increase in energy density due to sterile neutrino decays was found by calculating the energy produced by decays between active neutrino decoupling ($T \sim 1\,\mathrm{MeV}$) and photon decoupling ($T \sim 0.26\,\mathrm{eV}$). The BOOMERanG/MAXIMA constraint is shown in Figs. 7 and 8 and the potentially stringent future "constraints" by MAP and Planck are also shown.

C. Big bang nucleosynthesis

The energy density in the sterile neutrino sea at weak freeze-out just prior to primordial nucleosynthesis ($T \approx 0.7\,\mathrm{MeV}$) must not be too large. The energy density contribution of a sterile neutrino is often described as the fraction of the energy density in a fully populated (thermal) single neutrino-antineutrino species plus the energy density in the active neutrinos, N_ν. Depending on one's particular adoption of observationally inferred primordial abundances, one can arrive at limits between $N_\nu < 3.2$ and $N_\nu < 4$ [95–97]. We have calculated the energy density contributed by the sterile neutrino at BBN, and its limits are shown in Figs. 7 and 8.

D. ^{6}Li and D photoproduction

Another constraint arises from photoproduction of deuterium (D) and ^{6}Li stemming from the decay of massive sterile neutrinos after BBN [98]. Energetic cascades dissociate ^{4}He into excessive amounts of D, which is bounded observationally [99]. Also, energetic ^{3}H and ^{3}He produced in the cascades can synthesize ^{6}Li through $^3\mathrm{H}(^3\mathrm{He}) +^4\mathrm{He} \rightarrow^6\mathrm{Li} + \mathrm{n(p)}$, overproducing ^{6}Li, which is also bounded observationally [100].

These constraints lie in regions of parameter space which are almost identical to those bounded by CMB considerations. The ^{6}Li limit can be seen to extend to the small region just to the left of the CMB constraints in Figs. 7 and 8 (closely hatched area, hatching oriented from the lower right to the upper left). It should be noted that the ^{6}Li/D photoproduction constraints are from current observation, while the potential constraints from MAP and Planck of the energy density present at

CMB decoupling are a *future* possibility that can corroborate the photoproduction constraints.

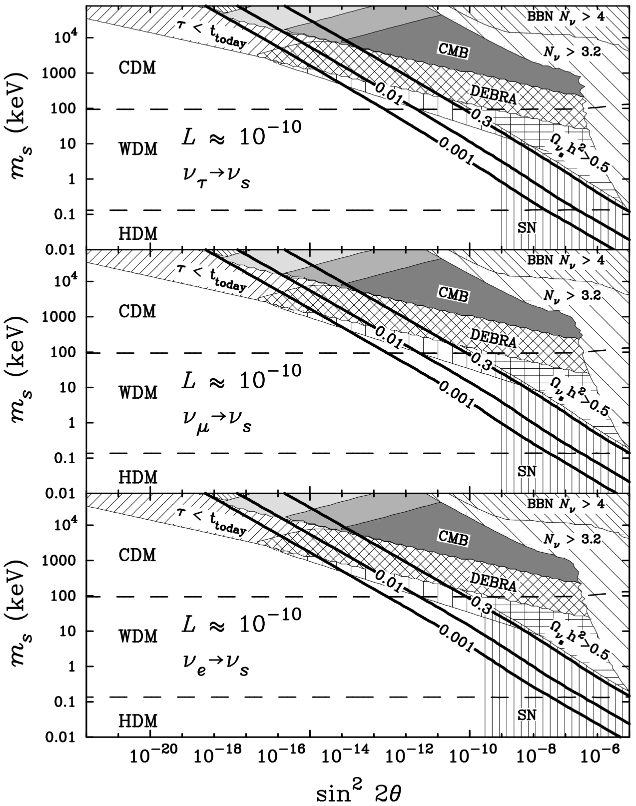

FIG. 7: Contours of closure fraction are displayed as thick lines labelled with $\Omega_{\nu_s} h^2$ for negligible lepton asymmetry ($L \approx 10^{-10}$) for the three neutrino flavors mixing with a massive sterile neutrino. Shown are constraints from the energy density present at CMB decoupling, with the dark gray region corresponding to BOOMERanG/MAXIMA's present limits. The medium gray region corresponds to MAP's predicted future constraint, and the light gray region is the Planck mission's potential constraint region. The constraints from DEBRA, and BBN are so labelled. The region of potential constraints from supernovae (SN) is also shown as closely spaced vertical lines. The region of widely spaced vertical lines is where radiative decays today may give detectable X-ray signatures. Regions filled with horizontal lines are where $\Omega_{\nu_s} h^2 > 0.5$ and are inconsistent with the observed age of the universe. Sterile neutrinos with parameters in the region labelled by "$\tau < t_{\rm today}$" decay without constrainable effects and make no contribution to the present matter density.

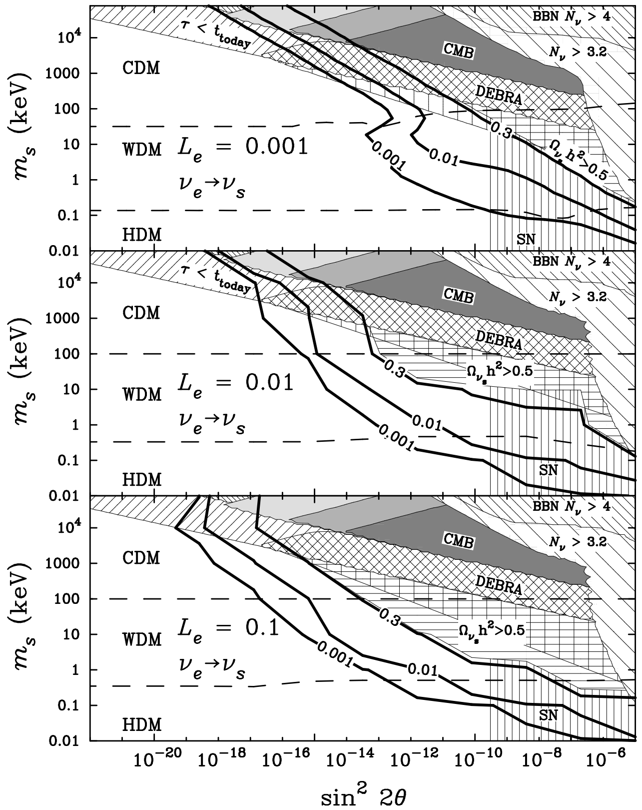

FIG. 8: Contours of closure fraction are displayed as thick lines labelled with $\Omega_{\nu_s} h^2$ for $L = 0.001, 0.01, 0.1$. Constraints are shown as in Fig. 7.

X. ACTIVE-STERILE NEUTRINO TRANSFORMATION IN CORE-COLLAPSE SUPERNOVAE

In the previous sections, we have calculated the ranges of sterile neutrino masses and mixing angles (and primordial lepton asymmetries) for which sterile neutrinos can account for some or all of the dark matter. In this section we describe some of the implications for core-collapse (Type Ib/c, II) supernovae of active-sterile neutrino transformation with parameters in these regions. Neutrinos play a dominant, pervasive role in core-collapse supernovae, so the stakes are high whenever we introduce non-standard neutrino physics like neutrino mixing.

In broad brush the effects are simple: too much neutrino conversion in a supernova results in too much energy loss to sterile neutrinos, manifestly in conflict with observation (the mixing angles considered here are sufficiently small that the sterile neutrinos are not trapped in the core). Requiring the hemorrhaging in sterile neutrinos not to be too great then places bounds on neutrino mixing parameters.

In fine detail, however, the procedure is not so simple, since the coupled supernova neutrino transport-transformation problem is highly nonlinear and the dynamics very difficult to treat analytically or numerically. Confounding the matter is our relatively poor understanding of the physics of the core-collapse phenomenon itself.

Nevertheless, we have boldly attempted (as have several workers before us [28, 29, 31, 68, 114]) to describe some of the salient effects of neutrino transformation in a supernova and have extracted some rather conservative limits on mixing parameters, conservative, at least, for arguing the case for sterile neutrino dark matter. Our "limits" are by no means final, and much future work remains to be done in order ascertain the viability of sterile neutrino dark matter. In what follows, we give a brief biography of a core-collapse supernova, describe the relevant neutrino transport and transformation physics, and indicate how we obtained the supernova "constraint" regions in Figs. 2, 3, 6, 7, and 8.

Core-collapse supernovae are the death throes of massive stars. A star of mass $\gtrsim 10 M_\odot$ dies when its $\approx 1.4 M_\odot$ iron core undergoes gravitational collapse to a neutron star, an event releasing $\approx 99\%$ of the $\approx 10^{53}$ erg gravitational binding energy of the neutron star in all active species of neutrinos (see Refs. [101, 102] for an introduction). In the standard picture this event lasts $\approx 10-15\,\mathrm{s}$ and can be divided roughly into three phases: the infall, shock reheating, and r-process epochs.

During the infall epoch, the iron core collapses on a near gravitational time scale of $\sim 1\,\mathrm{s}$ to a dense proto-neutron star. As the core density rises, the forward reaction in

$$e^- + \text{“}p\text{”} \rightleftharpoons \nu_e + \text{“}n\text{”} \tag{10.1}$$

neutronizes the core until the neutrino trapping density $\rho \sim 10^{11} - 10^{12}\,\mathrm{g\,cm^{-3}}$ is reached, a condition which allows the forward and reverse reactions in Eq. (10.1) to achieve β-equilibrium. This equilibrium is established with relativistically degenerate electrons ($\mu_e \approx 25 - 220\,\mathrm{MeV}$) and electron neutrinos ($\mu_{\nu_e} \approx 10 - 170\,\mathrm{MeV}$).

The quotes in Eq. (10.1) refer to free *and* bound baryons. Most of the baryons are bound in large nuclei, since the infall-collapse phase is characterized by temperatures $T \approx 1 - 3\,\mathrm{MeV}$ and a low entropy-per-baryon $s \approx 1.5$ (in units where Boltzmann's constant is unity).

The infall epoch ends when the core density reaches and exceeds the saturation density of nuclear matter. The inner core bounces, yielding an outward-propagating shock wave at its boundary with the outer core. The shock loses much of its energy dissociating the nuclei in the outer core and mantle of the pre-supernova star and eventually stalls some 500 km from the center of the core, far short of generating a supernova explosion. The post-bounce core is a hot, dense proto-neutron star consisting of free baryons, electrons and positrons, and active neutrino-antineutrino pairs (and perhaps also muon-antimuon pairs and strange quark matter), all in thermal and chemical equilibrium at a temperature $T \approx 30 - 70\,\mathrm{MeV}$ and entropy per baryon $s \approx 10$.

During the shock reheating epoch, at times post core bounce $t_{\rm pb} \approx 0.06 - 1\,\mathrm{s}$, neutrinos diffuse out of the core and deposit energy behind the stalled shock, driving the supernova explosion [103].

In the r-process epoch neutrinos continue to diffuse out of the star at times $t_{\rm pb} \approx 1 - 15\,\mathrm{s}$. The neutrinos drive mass loss from the proto-neutron star, possibly setting the physical conditions for r-process (heavy element) nucleosynthesis [104, 105].

The star's nuclear composition becomes increasingly neutron rich as the electron neutrinos depart the star and the reactions in Eq. (10.1) proceed with continuous, local re-establishment of β equilibrium. For example, at core bounce ($t_{\rm pb} = 0$), the electron fraction (net number of electrons per baryon) in the center of the core is $Y_e \approx 0.35$; a cold neutron star, the end point of evolution in this case, has $Y_e \lesssim 0.01$.

Since neutrinos dominate the energetics of core-collapse (Type Ib/c, II) supernovae, appreciable active-sterile neutrino transformation can completely alter the standard picture of stellar collapse. Although this picture has been refined by observations of neutrinos from SN 1987A [106], large-scale numerical simulations [103, 107], and semi-analytical work [103, 108–110], it is not clear that this is the only way for supernovae to evolve. Nevertheless, by requiring that not too much energy be "lost" too quickly to singlet neutrinos in the proto-neutron star, and hence avoiding a conflict with standard supernova theory and observations, we can delimit regions in the $m_s - \sin^2 2\theta$ plane which may adversely affect its evolution. In fact, many supernova constraints on new physics rely on limiting the energy loss to exotic particles in a proto-neutron star [111].

Sterile neutrinos can be produced in supernovae either coherently through mass level-crossings or incoherently via scattering-induced wave function collapse. Whether the former or latter process dominates depends on the hierarchy of length scales relevant for neutrino transport and transformation: the local neutrino mean free path λ, local neutrino oscillation length in matter l_m, and resonance width δr [the supernova analogue of Eq. (7.8)]. Neutrino flavor eigenstate evolution is coherent and transformation is uninterrupted through resonance if $\lambda \gg \delta r$. Neutrino flavor transformation is also adiabatic if $\delta r \gg l_m^{\rm res}$, where $l_m^{\rm res} \geq l_m$ is the oscillation length at resonance. This is in complete analogy to the evolution through resonances discussed above in Sec. VII for the early universe. If instead neutrino conversion is incoherent and transformation is interrupted often by collisions, then the conversion will be suppressed by quantum damping if $l_m > \lambda$.

It is easy to show that incoherent conversion dominates sterile neutrino production in supernova cores. In a proto-neutron star of radius $R = 10 - 50\,\mathrm{km}$ the density varies relatively slowly with distance from the center of the star, so the scale height of the weak potential is $H = |d \ln V/dr|^{-1} \approx 10 - 100\,\mathrm{km}$. Then the resonance width is $\delta r = H \tan 2\theta \approx (10^6 - 10^7\,\mathrm{cm}) \tan 2\theta$. The mean free path of a typical neutrino is about $\lambda \approx 10\,\mathrm{cm}$ (actually $\lambda \sim 10\,\mathrm{cm}$ to $\sim 10\,\mathrm{m}$, but this range makes little difference for our conclusions). Therefore, neutrino evolution is coherent if $\sin^2 2\theta \lesssim 10^{-12} - 10^{-10}$, and the maximal resonance width giving coherent evolution is $\delta r_{\rm max} \approx 10\,\mathrm{cm}$. Now the oscillation length at resonance is $l_m^{\rm res} = 4\pi E/\delta m^2 \sin 2\theta \approx 10^{-4}\,\mathrm{cm}\,(10\,\mathrm{keV}/m_s)^2/\sin 2\theta$, so coherent evolution gives $l_m^{\rm res} \gtrsim 10 - 100\,\mathrm{cm}\,(10\,\mathrm{keV}/m_s)^2$. In these conditions, however, the evolution is not adiabatic, since $\delta r_{\max} \lesssim l_m^{\rm res}$. As a result, mass level crossings contribute only subdominantly to sterile neutrino production in supernovae. Conversion to sterile neutrinos less massive than 10 keV is even less efficient, and more massive neutrinos will not have resonances.

Incoherent neutrino production is weakly damped at (or away from) a resonance when $\sin^2 2\theta \gtrsim 10^{-10}(10\,{\rm keV}/m_s)^4$. The local oscillation length in matter away from resonance is typically much smaller than the oscillation length at resonance, so for sterile neutrino masses $m_s \gtrsim 10\,{\rm eV}$ weak damping generally obtains off resonance even if the condition above is not met. Furthermore, since resonances last only a fraction $\lesssim 10^{-8}$ of the neutrino diffusion time scale, as derived below, most neutrino conversion in a core-collapse supernova occurs in the weak damping regime.

The time rate of energy "loss" $\mathcal{E}$ to sterile neutrinos (and sterile antineutrinos) per unit mass in a proto-neutron star is proportional to the active neutrino energy, scattering cross section on weak targets, and the average conversion probability [28, 29, 111]:

$$\begin{aligned}\mathcal{E} \approx \frac{1}{m_N}\int d\Phi_{\nu_\alpha} E\,\sigma_{\nu_\alpha}(E)\frac{1}{2}\langle P_m(\nu_\alpha\to\nu_s;p,t)\rangle \\ +\frac{1}{m_N}\int d\Phi_{\bar\nu_\alpha} E\,\sigma_{\bar\nu_\alpha}(E)\frac{1}{2}\langle P_m(\bar\nu_\alpha\to\bar\nu_s;p,t)\rangle,\end{aligned} \tag{10.2}$$

where, for the sake of simplicity, we have suppressed Pauli-blocking effects. In Eq. (10.2), the cross sections for neutrino scattering on free baryons are $\sigma_{\nu_\alpha}(E) \approx \sigma_{\bar\nu_\alpha}(E) \approx 1.66 G_F^2 E^2$, and the differential neutrino and antineutrino fluxes are

$$\begin{aligned} d\Phi_{\nu_\alpha} &= c\,dn_{\nu_\alpha} \approx \frac{d^3p}{(2\pi)^3}\frac{1}{e^{E/T_{\nu_\alpha}-\eta_{\nu_\alpha}}+1} \\ &\approx \frac{1}{2\pi^2}\frac{E^2 dE}{e^{E/T_{\nu_\alpha}-\eta_{\nu_\alpha}}+1}\end{aligned} \tag{10.3}$$

$$\begin{aligned} d\Phi_{\bar\nu_\alpha} &= c\,dn_{\nu_\alpha} \approx \frac{d^3p}{(2\pi)^3}\frac{1}{e^{E/T_{\bar\nu_\alpha}-\eta_{\bar\nu_\alpha}}+1} \\ &\approx \frac{1}{2\pi^2}\frac{E^2 dE}{e^{E/T_{\bar\nu_\alpha}-\eta_{\bar\nu_\alpha}}+1}\end{aligned} \tag{10.4}$$

for relativistic neutrinos, where $\eta_{\nu_\alpha} = \mu_{\nu_\alpha}/T_{\nu_\alpha}$ is the denegeracy parameter of ν_α as above. A simple but somewhat crude criterion for avoiding conflict with supernova theory and observations of SN 1987A is $\mathcal{E} \lesssim 10^{19}\,{\rm erg\,s^{-1}\,g^{-1}}$ [111], a limit on the sterile neutrino emissivity equivalent to a loss of $\sim 10\,{\rm MeV}$ per baryon per second.

The weak potentials [cf. Eqs. (5.5) and (5.6)] which drive neutrino flavor transformation take a slightly different form in supernovae than in the early universe [64]. For $\nu_e \rightleftharpoons \nu_s$ transformation the potential stemming from finite density effects is [from Eq. (5.5)]

$$V^D = \frac{G_F\rho}{\sqrt{2}m_N}\left(3Y_e - 1 + 4Y_{\nu_e} + 2Y_{\nu_\mu} + 2Y_{\nu_\tau}\right), \tag{10.5}$$

where $m_N \approx 931.5\,{\rm MeV}$ is an atomic mass unit, n_i is the number density of species i, and $Y_i \equiv (n_i - n_{\bar i})/n_B$ is the net fraction of species i per baryon ($n_B = n_n + n_p$). In part, the form of Eq. (10.5) follows from local charge neutrality and the assumption that muons, anti-muons, and strange quark matter are negligibly populated. The finite density potential for $\nu_\mu \rightleftharpoons \nu_s$ transformation is [from Eq. (5.5)]

$$V^D = \frac{G_F\rho}{\sqrt{2}m_N}\left(Y_e - 1 + 2Y_{\nu_e} + 4Y_{\nu_\mu} + 2Y_{\nu_\tau}\right). \tag{10.6}$$

The potential for $\nu_\tau \rightleftharpoons \nu_s$ transformation follows from Eq. (10.6) upon switching the labels ν_μ and ν_τ. The finite temperature potential V^T is negligible in supernovae [64], so the total potentials for neutrino and antineutrino transformation are $V = V^D + V^T \approx V^D$ and $\bar V = -V^D + V^T \approx -V^D \approx -V$, respectively.

The average oscillation probabilities in Eq. (10.2) depend on the weak potentials and neutrino mixing parameters, from Eqs. (6.4), (6.5):

$$\begin{aligned}&\langle P_m(\nu_\alpha\to\nu_s;p.t)\rangle \approx \\ &\quad\frac{1}{2}\frac{\Delta(E)^2\sin^2 2\theta}{\Delta(E)^2\sin^2 2\theta + D^2 + [\Delta(E)\cos 2\theta - V^D]^2}\end{aligned} \tag{10.7}$$

$$\begin{aligned}&\langle P_m(\bar\nu_\alpha\to\bar\nu_s;p,t)\rangle \approx \\ &\quad\frac{1}{2}\frac{\Delta(E)^2\sin^2 2\theta}{\Delta(E)^2\sin^2 2\theta + \bar D^2 + [\Delta(E)\cos 2\theta + V^D]^2},\end{aligned} \tag{10.8}$$

where $\Delta(p) = \delta m^2/2p \approx m_s^2/2E \approx \Delta(E)$ for relativistic neutrinos. As before the quantum damping rate $D = \Gamma_{\nu_\alpha}/2 = \int d\Phi_{\nu_\alpha}\sigma_{\nu_\alpha}(E)/2$ for neutrinos is one-half the neutrino scattering rate; an analogous expression applies for the antineutrino damping rate $\bar D$. The coherent effects described in Ref. [69] may modify these conversion rates.

The conditions for resonance $\pm V^D = \Delta(p)\cos 2\theta \approx m_s^2\cos 2\theta/2E$, the potentials in Eqs. (10.5), (10.6), and the average oscillation probabilities in Eqs. (10.7), (10.8) imply a negative feedback between active (anti)neutrino transformation and the potentials. If quantum damping effects are comparable for neutrinos and antineutrinos or are relatively unimportant, as argued above for most of the parameter range of interest, neutrino conversion is enhanced relative to antineutrino conversion when $V^D > 0$. The preferential conversion of neutrinos *decreases* the potential, since the finite density part of the potential depends on the relative excess (or deficit) of particles over antiparticles (the net contribution of particle-antiparticle pairs is zero). As the potential decreases, the neutrino and antineutrino conversion rates approach the common rate they would have at vanishing potential. Since neutrinos and antineutrinos of all flavors are produced in roughly equal numbers and their individual number densities are at least comparable to the electron density, the dynamical feedback mechanism may drive the potential V^D locally to zero throughout the proto-neutron star, as long as the time scale for this process is less than the local neutrino diffusion time scale $t_d \sim \lambda(R/\lambda)^2/c \sim 3\,\mathrm{s}$; a similar sequence will ensue if $V^D < 0$. If this happens, the equal neutrino and antineutrino conversion rates ensure that the potential will remain zero, with any local deviation continuously smoothed out, up to the higher order effects of neutrino diffusion.

In this sense zero potential is a fixed point of the dynamics of neutrino transport and conversion in core-collapse supernovae and the time scale for achieving zero potential is a dynamical equilibration time scale. The situation is more complicated if sterile neutrinos mix with multiple active neutrinos or if damping is important. For example, an excess of neutrinos over antineutrinos implies damping is asymmetric, and this can retard equilibration. These issues will be examined in more detail in a separate work [112]. We note in passing that this behavior can also occur when neutrino scattering is rare and mass level crossings dominate sterile neutrino production [113]; some of this physics has also been discussed in connection with active-active neutrino transformation in proto-neutron stars [114].

We can estimate the equilibration time scale τ_V for driving a potential V_0^D to zero by computing the time over which the disparity in the rates of neutrino and antineutrino conversion will induce a potential $\delta V^D = -V_0^D$ which cancels the original potential V_0^D. Now Eqs. (10.5), (10.6) imply $\delta V^D = 2\sqrt{2}G_F(\delta n_{\nu_\alpha} - \delta n_{\bar{\nu}_\alpha})$, where δn_{ν_α} and $\delta n_{\bar{\nu}_\alpha}$ are the numbers of neutrinos and antineutrinos converted per unit volume, respectively. The number densities of (anti)neutrinos converted are proportional to the rates of (anti)neutrino conversion per baryon, the baryon density, and the time over which the conversion takes place. If we assume τ_V is small compared to the time scales for the change of the density and temperature in the star (a "static" approximation), we have $\delta n_{\nu_\alpha} = -n_B \tau_V \int d\Phi_{\nu_\alpha} \sigma_{\nu_\mu}(E) \frac{1}{2}\langle P_m(\nu_\mu \to \nu_s; p, t)\rangle$ and similarly for $\delta n_{\bar{\nu}_\alpha}$. Solving for τ_V and using $n_B = \rho/m_N$ gives the time scale for achieving dynamic equilibrium in the $\nu_\alpha \rightleftharpoons \nu_s$, $\bar{\nu}_\alpha \rightleftharpoons \bar{\nu}_s$ system:

$$\tau_V = \frac{V_0^D m_N}{2\sqrt{2}G_F\rho}\left(\int d\Phi_{\nu_\alpha}\sigma_{\nu_\alpha}(E)\frac{1}{2}\langle P_m(\nu_\alpha \to \nu_s; p, t)\rangle \right.$$
$$\left. - \int d\Phi_{\bar{\nu}_\alpha}\sigma_{\bar{\nu}_\alpha}(E)\frac{1}{2}\langle P_m(\bar{\nu}_\alpha \to \bar{\nu}_s; p, t)\rangle\right)^{-1}. \quad (10.9)$$

It is instructive to evalute the equilibration time scale τ_V for the $\nu_\mu \rightleftharpoons \nu_s$, $\bar{\nu}_\mu \rightleftharpoons \bar{\nu}_s$ system in two limits: (i) far away form a resonance, for which $|V_0^D| \gg \Delta(E)\cos 2\theta$; and (ii) very near or at a resonance, where $|V_0^D| \approx \Delta(E)\cos 2\theta \approx m_s^2/2E$ for $\theta \ll 1$. In the off-resonance case, inserting Eqs. (10.3)-(10.4) and Eqs. (10.7)-(10.8) in Eq. (10.9) and expanding to lowest order yields

$$\begin{aligned}\tau_V^{\mathrm{off-res}} &\approx \frac{96}{1.66\sqrt{2}}\frac{\left(V_0^D\right)^4 m_N}{G_F^3\rho T^2 m_s^6 \sin^2 2\theta} \\ &\approx \frac{1.5\times 10^{-8}\,\mathrm{s}}{\sin^2 2\theta}\left(\frac{10^{14}\,\mathrm{g\,cm^{-3}}}{\rho}\right) \\ &\times \left(\frac{50\,\mathrm{MeV}}{T}\right)^2\left(\frac{10\,\mathrm{keV}}{m_s}\right)^6\left(\frac{V_0^D}{1\,\mathrm{eV}}\right)^4,\end{aligned} \quad (10.10)$$

where the factor of 1.66 comes from the neutrino scattering cross section given earlier. We have derived Eq. (10.10) by assuming a locally constant density and temperature, consistent with our "static" approximation. We have also ignored the build up of a non-zero muon neutrino chemical potential μ_{ν_μ} and accompanying Pauli blocking in neutrino scattering and pair production as equilibration proceeds, a simplification giving $d\Phi_{\nu_\mu} \approx d\Phi_{\bar{\nu}_\mu}$. Using the same simplifications, we can find the time scale in the on-resonance case:

$$\begin{aligned}\tau_V^{\mathrm{on-res}} &\approx \frac{8\pi^2}{(1.66)45\sqrt{2}\zeta(5)}\frac{|V_0^D|m_N}{G_F^3\rho T^5} \\ &\approx \frac{16\zeta(3)}{(1.66)7\pi^2\sqrt{2}\zeta(5)}\frac{m_s^2 m_N}{G_F^3\rho T^6} \\ &\approx 2\times 10^{-9}\,\mathrm{s}\left(\frac{50\,\mathrm{MeV}}{T}\right)^5\left(\frac{10^{14}\,\mathrm{g\,cm^{-3}}}{\rho}\right)\left|\frac{V_0^D}{1\,\mathrm{eV}}\right| \\ &\approx 6.6\times 10^{-10}\,\mathrm{s}\left(\frac{50\,\mathrm{MeV}}{T}\right)^6\left(\frac{10^{14}\,\mathrm{g\,cm^{-3}}}{\rho}\right) \\ &\times \left(\frac{m_s}{10\,\mathrm{keV}}\right)^2.\end{aligned} \quad (10.11)$$

The second and fourth expressions of Eq. (10.11) follow from the resonance condition $|V_0^D| \approx m_s^2/2E$ and taking the neutrino energy E to be the average neutrino energy $\langle E\rangle = \int d\Phi_{\nu_\mu}E/\int d\Phi_{\nu_\mu} \approx 7\pi^4 T_{\nu_\mu}/180\zeta(3) \approx 3.15 T_{\nu_\mu}$ in the proto-neutron star.

The on- and off-resonance equilibration time scales both vary inversely with the ambient density and temperature. Hotter conditions enhance the neutrino conversion rate per scatterer, and denser conditions enhance the number density of scatterers. In either case it takes less time to drive a pre-existing potential to zero. On the other hand, only the off-resonance time scale $\tau_V^{\mathrm{off-res}}$ depends on the vacuum mixing angle; the inverse dependence is natural, since the emissivity in sterile (anti)neutrinos is proportional to $\sin^2 2\theta$. The on-resonance time scale $\tau_V^{\mathrm{on-res}}$ is independent of $\sin^2 2\theta$, because the relevant mixing angle at a resonance is $\pi/4$. If $V_0^D > 0$ neutrino conversion dominates antineutrino conversion at resonance and vice versa if $V_0^D < 0$, so this time scale is extremely short compared to the neutrino diffusion time scale or indeed *any* time scale typically associated with a core-collapse supernova. Individual resonances are fleeting and result in negligible energy loss to sterile neutrinos. As a result, we may safely assume that most neutrino transformation takes place off resonance, with an equilibration time scale given by Eq. (10.10).

We can delimit ranges of the neutrino mixing parameters m_s and $\sin^2 2\theta$ which *may* adversely affect core-collapse supernovae by evaluating the sterile neutrino emissivity in Eq. (10.2) in the following manner.

In the case of $\nu_e \rightleftharpoons \nu_s$ transformation, the potential V^D is initially positive in the post-bounce supernova core. If the neutrino mixing parameters happen to give $\tau_V^{\rm off-res} > t_d$, core neutronization proceeds roughly on a diffusion time scale, although the conversion of electron neutrinos accelerates the shift of β equilibrium toward neutron richness. Neutronization decreases the electron fraction Y_e, and neutrino conversion decreases the electron neutrino fraction Y_{ν_e}. As a consequence, the potential decreases and eventually reaches a value such that $\tau_V^{\rm off-res} < t_d$.

Once this occurs, neutrino conversion quickly resets the potential to zero and maintains this value as neutronization continues. If instead the neutrino mixing parameters happen to give $\tau_V^{\rm off-res} < t_d$ at core bounce, conversion immediately resets and maintains the potential at zero.

In the case of $\nu_\mu \rightleftharpoons \nu_s$ or $\nu_\tau \rightleftharpoons \nu_s$ transformation, the potential V^D is initially *negative* in the post-bounce core. Here conversion has no direct effect on the rate of neutronization (notwithstanding feedback on the nuclear equation of state), which increases the magnitude of the potential as the electron fraction falls to a value ~ 0.01. Unless $\tau_V^{\rm off-res} < t_d$ from the outset, neutronization dictates the evolution of the potential.

The emissivity $\mathcal{E}$ depends on the local, instantaneous value of the potential, so the total energy lost to sterile neutrinos depends on the time history of the spatially varying potential and, in particular, whether neutronization or neutrino conversion locally dominates its evolution. An accurate estimate of the spatially integrated emissivity and, hence, of the regions in parameter space which may alter the standard picture of stellar collapse clearly requires a detailed investigation of the dynamics of these systems, as well as a better understanding of the physics of core-collapse supernovae.

From the viewpoint of the viability of sterile neutrinos as dark matter, however, we may *conservatively* estimate the emissivity by assuming the system achieves zero potential relatively quickly, so that $\mathcal{E}$ is evaluated with $V^D = 0$. Evaluating Eq. (10.2) in this limit and imposing the condition $\mathcal{E} \lesssim 10^{19}\,{\rm erg\,s^{-1}\,g^{-1}}$ gives the disfavored regions $\sin^2 2\theta \gtrsim 3\times10^{-10}$ for $\nu_e \rightleftharpoons \nu_s$ transformation and $\sin^2 2\theta \gtrsim 10^{-9}$ for $\nu_\mu \rightleftharpoons \nu_s$ or $\nu_\tau \rightleftharpoons \nu_s$ transformation for sterile neutrino masses $m_s \gtrsim 10\,{\rm eV}$. For smaller masses, the limits are significantly weaker, owing to the onset of quantum damping. These limits are shown in Figs. 2, 3, 6, 7, and 8. The emissivity falls with increasing potential away from a resonance, so more detailed future work on this complex problem may find actual constraints which are weaker than the very conservative limits given here.

Sterile neutrino dark matter parameters which lie near the edges of the disfavored regions in Figs. 2, 3, 6, 7, and 8 could give interesting signals in current and future supernova neutrino detectors (see, *e.g.*, Ref. [115]). These detectors possibly could discern unique signatures for sterile neutrinos. Such signatures would bolster the case for sterile neutrino dark matter.

To summarize this section, we have delimited conservatively the regions in the parameter space of active-sterile neutrino mixing that are disfavored by energy-loss considerations in core-collapse supernovae. We have found that the coupled problem of neutrino transport and flavor transformation in hot and dense nuclear matter is a formidable one. It involves following the local evolution of the weak potential which drives flavor transformation, including the feedback from diffusion and the conversion itself. We have described this physics roughly by estimating the competing time scales for lepton number diffusion and for cancellation of the potential. Depending on the mixing parameters and the spacetime evolution of the potential, the potential may well be reset to zero in much of the proto-neutron star, so the effects of neutrino propagation in matter need not suppress sterile neutrino (or antineutrino) production. As a result, core-collapse supernovae can be significantly more sensitive to active-sterile neutrino mixing than they were found to be in previous studies [28, 31, 68]. These studies used a spatially and temporally constant value of the potential, resulting in limits on mixing angles similar to ours but for significantly larger sterile neutrino masses $\gtrsim 10\,{\rm keV}$; for smaller masses their limits on mixing angles are weaker because the putative matter effects suppress conversion [28, 31, 68].

Of course, we have deliberately chosen to be conservative in applying supernova limits, since our objective in this work is to assess the viability of sterile neutrino dark matter. The true limits, quite interesting in their own right and obtained from a self-consistent and proper treatment of the full, multi-dimensional Boltzmann evolution of the neutrino seas coupled with the nuclear equation of state, may well lie somewhere in between the values determined in this and previous studies. We leave attempts at such investigations for a future work [112].

XI. CONCLUSIONS

We have estimated the resonant and non-resonant scattering prodution of sterile neutrinos in the early universe. The basis for the production of these sterile species is a presumed mixing with active neutrinos in vacuum. Of course, such mixing renders these species not truly "sterile." As a result, the "sterile" neutrinos can decay and this, together with their overall contribution to energy density, constitutes the basis for several stringent cosmological and astrophysical constraints which we have discussed in detail.

Additionally, these sterile species may produce significant effects in core-collapse supernovae. Some of these effects, such as massive core energy loss, could be the basis for true constraints. However, it must be kept in mind that (1) the supernova explosion energy is only some $\sim 1\%$ of the total energy resident in the active neutrino seas and that (2) we do not yet understand in detail how supernovae explode (nor do we have a sufficiently detailed observed core-collapse neutrino signal to place stringent constraints). Better theoretical understanding of supernova physics, perhaps coupled with the neutrino signature of a Galactic core-collapse event, may allow the indicated regions on Figs. 7 and 8 to become true hard and fast constraints instead of simply "disfavored" parameter regions. In fact, deeper insight into the time evolution of the potentials governing sterile neutrino production in the core may allow *extension* of the constrained parameter region to even smaller values of vacuum mixing angle.

Nevertheless, it is clear from our work that sterile "neutrino" species with ranges of masses and vacuum couplings could be produced in quantities sufficient to explain *all* of the non-baryonic dark matter, while evading all present day laboratory and astrophysical constraints. Within the allowed ranges in mass and mixing parameters which give these dark matter solutions are regions where the sterile neutrino masses and/or energy spectra combine to produce collisionless damping scales corresponding to warm or even cold dark matter, subsuming the interesting behavior range for large scale structure.

It is then a disturbing possibility that the dark matter might not be "weakly interacting massive particles" (WIMPs), but rather "nearly non-interacting massive particles" (NNIMPs) which are likely not detectable in ordinary dark matter detection experiments. This possibility begs two questions: (1) how could we hope to constrain or definitively detect this dark matter candidate; and (2) what are sterile neutrinos?

The answer to the first question is more straightforward than the resolution of the second. As outlined above, better understanding of the neutrino and equation of state physics of core-collapse supernovae could help us extend constraints. Improved observations and models of x-ray emission from clusters of galaxies and other objects could provide stringent constraints or, conceivably, even detections of sterile neutrino photon decay.

As discussed above, future observations bearing on the clustering of dwarf galaxy or Lyman-α cloud halos at high redshift may provide evidence for or against WDM as opposed to CDM. Direct evidence for WDM would constitute a point in favor of sterile neutrinos, though not a definitive one by any means. Likewise, and insidiously, our allowed parameter space for dark matter accommodates standard CDM behavior, even for lepton numbers equal to the baryon number.

Direct detection of WIMPs in the laboratory or detection of gamma rays associated with WIMP annihilation in galactic centers [116] obviously rule out sterile neutrino dark matter, given the small vacuum mixing angles suggested by our work. It is worth considering whether β-decay electron energy spectrum or pion decay experiments could be pushed in sensitivity to the point where massive sterile neutrinos in some of the allowed regions of Figs. 7 and 8 could be constrained. This would require an increase in sensitivity to $m_s \sin^2 2\theta$ of at least some six orders of magnitude and this is clearly untenable with *current* technology [33]. Finally, although a number of extensions of the standard model motivate the existence of multiple sterile neutrinos, it must be pointed out there is no independent physics suggestion for the sterile neutrino mass ($\sim 1\,\mathrm{keV}$ to $\sim 10\,\mathrm{MeV}$) and mixing ($10^{-17} \leq \sin^2 2\theta \leq 3 \times 10^{-10}$) parameters which give viable dark matter candidates in our calculations.

As discussed above, sterile neutrino degrees of freedom with ultra-large masses (*e.g.*, of order the standard model unification scale, or even the top quark mass) are in some sense "natural," at least in the context of a see-saw explanation for the low masses of active neutrinos.

There is now a *reasonable* chance that new neutrino experiments scheduled to come to fruition in the next few years [*e.g.*, the Sudbury Neutrino Observatory (SNO) [117], KamLAND [118], ORLaND [119], K2K [120], MINOS [121], ICARUS [122], and Mini-BooNE [123]] will allow us to deconvolve the neutrino mass and mixing spectrum. This would be an achievement heavy with implications for many aspects of physics and astrophysics. Will the requirement for sterile neutrinos remain?

It is now true that the interpretation of the current solar, atmospheric, and accelerator (LSND) data in terms of neutrino flavor mixing physics demands the introduction of a sterile neutrino with a rest mass comparable to that of some of the active neutrinos, *i.e.*, light. Necessarily, then, this sterile neutrino is not the dark matter candidate we speculate on in this work. However, the unambiguous establishment of the existence of a light sterile neutrino would expose our ignorance of physics in the neutrino sector in a stark and dramatic way. On this score, the Mini-BooNE experiment [123] and the SNO neutral-current experiment [117] are the most crucial ones for sterile neutrino dark matter. A confirmation of the LSND result invites speculation on the existence of more massive sterile neutrino states.

ACKNOWLEDGMENTS

We thank A.B. Balantekin, J. Behr, S. Burles, D.O. Caldwell, J. Frieman, E. Gawiser, K. Griest, W. Haxton, C. Hogan, E.W. Kolb, R.N. Mohapatra, S. Reddy, R. Rothschild, B. Sadoulet, D. Tytler, and J. Wadsley for useful discussions. M.P. and K.A. would like to acknowledge partial support from NASA GSRP. This work was supported in part by NSF Grant PHY-9800980 at UCSD. G.M.F. would like to thank the Institue for Nuclear Theory, the Physics Department, and the Astronomy Department of the University of Washington for hospitality.

APPENDIX: THE GENERAL TIME-TEMPERATURE RELATION

In this appendix, we review the calculation of the temperature evolution in the early universe through periods of varying statistical weight in relativistic particles, g, Eq. (7.6). The time derivative of the temperature can be written as [124]

$$\frac{dT}{dt} = \frac{dr}{dt} \bigg/ \frac{dr}{dT} \tag{1}$$

where $r \equiv \ln(R^3)$ and R is the scale factor. The expansion rate is determined by the Friedmann equation

$$H = \frac{dR}{dt}\frac{1}{R} = \frac{1}{m_{\rm pl}}\sqrt{\frac{8\pi}{3}\rho_{\rm tot}} \approx 0.207\,{\rm s}^{-1}\; g^{1/2}\; T^2, \tag{2}$$

where $\rho_{\rm tot} = (\pi^2/30)gT^4$ is the total energy density, and T is in MeV in the last approximation of Eq. (2). Therefore, the first half of the time-temperature relation, Eq. (1), is straightforward: $dr/dt = 3H$. One can get the second half through the conservation of comoving energy,

$$\frac{d}{dt}\left(\rho R^3\right) + p\frac{d}{dt}\left(R^3\right) = 0 \tag{3}$$

This can be rewritten into the desired form

$$\frac{dr}{dT} = \frac{d\rho_{\rm tot}}{dT}\left(\rho_{\rm tot} + p_{\rm tot}\right)^{-1}. \tag{4}$$

With Eqs. (2) and (4) one has the general temperature evolution.

In our case the sterile neutrinos can contribute significantly to the energy density and pressure. Approximating all species other than the sterile neutrino to be relativistic, we have $p_* \approx 1/3\rho_*$, where ρ_* and p_* are the energy and pressure in all particles other that the sterile neutrinos/antineutrinos. Therefore,

$$\frac{dT}{dr} = \left(\frac{4}{3}\rho_* + \rho_s + p_s\right)\left(\frac{d\rho_*}{dT} + \frac{d\rho_s}{dT}\right)^{-1}. \tag{5}$$

The rate of change of the standard energy density is straightforward:

$$\frac{d\rho_*}{dT} = \frac{4\pi^2}{30}gT^3 + \frac{\pi^2}{30}T^4\frac{dg}{dT}. \tag{6}$$

The temperature derivative of the sterile neutrino energy density is

$$\begin{aligned}\frac{d\rho_s}{dT} &= \frac{2}{\pi^2}\int\left(f_{\nu_s}(p) + f_{\bar\nu_s}(p)\right)\left[(p^2+m_s^2)/T^2\right]^{1/2}p^2dp\\ &- \frac{m_s^2}{2\pi^2}\int\left[f_{\nu_s}(p) + f_{\bar\nu_s}(p)\right]\left[(p^2+m_s^2)/T^2\right]^{-1/2}p^2dp.\end{aligned}$$

This, together with the energy density and pressure in the sterile neutrinos and antineutrinos calculated from their time-dependent distribution functions, allows one to readily arrive at a consistent time-temperature evolution.

REFERENCES

[1] M. Gell-Mann, P. Ramond, and R. Slansky, in *Supergravity*, edited by P. van Nieuwenhuizen and D.Z. Freedman (North-Holland, Amsterdam, 1979); T. Yanagida, in *Proceedings of the Workshop on Unified Theories and Baryon Number in the Universe*, edited by A. Sawada and A. Sugamoto, K.E.K. preprint 79-18 (1979); R.N. Mohapatra and G. Senjanovic, Phys. Rev. Lett. **44**, 912 (1980).

[2] Y. Fukuda *et al.* (Super-Kamiokande Coll.), Phys. Rev. Lett. **81**, 1562 (1998).

[3] T.J. Haines *et al.* (IMB Coll.), Phys. Rev. Lett. **57**, 1986 (1986).

[4] R. Davis, D.S. Harmer, and K.C. Hoffman, Phys. Rev. Lett. **21**, 1205 (1968).

[5] J.N. Bahcall, P. Krastev, and A.Yu. Smirnov, Phys. Rev. D **58**, 096016 (1998); M.C. Gonzalez-Garcia, M. Maltoni, C. Peña-Garay, and J.W.F. Valle, to appear, Phys. Rev. D, hep-ph/0009350, and references therein.

[6] C. Athanassopoulos *et al.*, Phys. Rev. Lett. **75**, 2650 (1996); **77**, 3082 (1996); **81**, 1774 (1998); Phys. Rev. C **54**, 2685 (1996); **58**, 2489 (1998).

[7] D.E. Groom *et al*, Eur. Phys. J. **C15**, 1 (2000).

[8] G.M. Fuller and R.A. Malaney, Phys. Rev. D **43**, 3136 (1991).

[9] E.W. Kolb and M.S. Turner, Phys. Rev. Lett. **67**, 5 (1991).

[10] S. Dodelson and L.M. Widrow, Phys. Rev. Lett. **72**, 17 (1994).

[11] X. Shi and G.M. Fuller, Phys. Rev. Lett. **82**, 2832 (1999).

[12] S.P. Mikheyev and A.Yu. Smirnov, Yad. Fiz. **42**, 1441 (1985) [Sov. J. Nucl. Phys. **42**, 913 (1985)]; L. Wolfenstein, Phys. Rev. D **17**, 2369 (1978).

[13] A.B. Balantekin, J.F. Beacom and J.M. Fetter, Phys. Lett. **B 427**, 317 (1998); A.B. Balantekin and J.F. Beacom, Phys. Rev. D **54**, 6323 (1996).

[14] B. Zeitnitz *et al.*, Prog. Part. Nucl. Phys. **40**, 169 (1998); B. Armbruster *et al.*, Phys. Rev. C **57**, 3414 (1998); K. Eitel and B. Zeitnitz, Nucl. Phys. Proc. Suppl. **77**, 212 (1999).

[15] C. Eitel, New J. Phys. **2**, 1 (2000).

[16] P.F. Harrison, D.H. Perkins, and W.G. Scott, Phys. Lett. **B349**, 137 (1995); **B396**, 186 (1997).

[17] C.Y. Cardall and G.M. Fuller, Phys. Rev. D **53**, 4421 (1996).

[18] V. Barger, Y. Dai, K. Whisnant and B. Young, Phys. Rev. D **59**, 113010 (1999).

[19] A. Acker and S. Pakvasa, Phys. Lett. **B397**, 209 (1997).

[20] P. Langacker, Phys. Rev. D**58**, 093017 (1998).

[21] N. Arkani-Hamed and Y. Grossman, Phys. Lett. **B459**, 179 (1999).

[22] E.J. Chun and H.B. Kim, Phys. Rev. D **60**, 095006 (1999).

[23] J.C. Romão *et al.*, Phys. Rev. D **61**, 071703 (2000); M. Hirsch *et al.*, Phys. Rev. D **62**, 113008 (2000); J.C. Romão, talk given at the NATO Advanced Study Institute 2000, Cascais, Portugal, 26 June - 7 July 2000, hep-ph/0011351.

[24] R.J. Lindebaum, G.B. Tupper, and R.D. Viollier, Mod. Phys. Lett. **A15**, 1221 (2000).

[25] N. Arkani-Hamed, S. Dimopoulos, and G. Dvali, hep-ph/9811448; K.R. Dienes, E. Dudas, and T. Gherghetta, Nucl. Phys. **B557**, 25 (1999); K.R. Dienes and I. Sarcevic, Phys. Lett. **B500**, 133 (2001); G. Dvali and A.Yu. Smirnov, Nucl. Phys. **B563**, 63 (1999); R.N. Mohapatra, S. Nandi, and A. Pérez-Lorenzana, Phys. Lett. **B466**, 115 (1999); R.N. Mohapatra and A. Pérez-Lorenzana, Nucl. Phys. **B576**, 466 (2000); R. Barbieri, P. Creminelli, and A. Strumia, *ibid.* **B585**, 28 (2000); A. Lukas, P. Ramond, A. Romanino, and G.G. Ross, Phys. Lett. **B495**, 136 (2000); *ibid.*, hep-ph/0011295; R.N. Mohapatra and A. Pérez-Lorenzana, hep-ph/0006278; N. Cosme *et al.*, Phys. Rev. D (to be published), hep-ph/0010192; D.O. Caldwell, R.N. Mohapatra, and S. J. Yellin, hep-ph/0010353; *ibid.*, hep-ph/0102279.

[26] K. Abazajian, G.M. Fuller, and M. Patel, hep-ph/0011048.

[27] M.T. Ressell and M.S. Turner, Comments Astrophys. **14**, 323 (1989).

[28] K. Kainulainen, J. Maalampi, and J.T. Peltoniemi, Nucl. Phys. **B358**, 435 (1991); A.D. Dolgov, S.H. Hansen, G. Raffelt, D.V. Semikoz, Nucl. Phys. **B580**, 331 (2000).

[29] G. Raffelt and G. Sigl, Astropart. Phys. **1**, 165 (1993).

[30] G.M. Fuller, lectures at the XXVIII SLAC Summer Institute on Particle Physics: Neutrinos from the Lab, the Sun, and the Cosmos, August 14-25, 2000, http://www.slac.stanford.edu/gen/meeting/ssi/2000/fuller.html.

[31] A.D. Dolgov, S.H. Hansen, G. Raffelt, and D.V. Semikoz, Nucl. Phys. **B590**, 562 (2000).

[32] D.I. Britton *et al.*, Phys. Rev. D **46**, R885 (1992); D.I. Britton *et al.*, Phys. Rev. Lett. **68**, 3000 (1992); D.I. Britton *et al.*, Phys. Rev. D **49**, 28 (1994); D.A. Bryman and T. Numao, Phys. Rev. D. **53**, 558 (1996).

[33] J. Behr, private communication; A. Gorelov *et al.*, Hyperfine Interactions **127**, 373 (2000); M. Trinczek *et al.*, to be published.

[34] P. Astier *et al.* [NOMAD Collaboration], Phys. Lett. B **506**, 27 (2001) [hep-ex/0101041].

[35] B. Moore *et al.*, Astrophys. J. Lett., **524**, L19 (1999) [astro-ph/9907411]; S. Ghigna *et al.*, Astrophys. J. **544**, 616 (2000) [astro-ph/9910166].

[36] M. Mateo, Ann. Rev. As. & Atrophys. **36**, 435 (1998).

[37] J.R. Primack, astro-ph/0007187; J.R. Primack, Nucl. Phys. Proc. Suppl. **87**, 3 (2000)

[38] A.M. Wolfe and J.X. Prochaska, Astrophys. J. **545**, 591 (2000); *ibid.*, 603 (2000); *ibid.*, **494**, L15 (1998); J.X. Prochaska and A.M. Wolfe, *ibid.*, **487**, 73 (1997).

[39] F.C van den Bosch *et al.*, Astron. J. **119**, 1579 (2000); F.C. van den Bosch and R. Swaters, submitted to Astron. J., astro-ph/0006048; A. Borriello and P. Salucci, submitted to Mon. Not. R. Astron. Soc., astro-ph/0001082; A. Burkert, Astrophys. J. Lett. **474**, L99 (1997).

[40] B. Moore *et al.*, Astrophys. J. **499**, L5 (1998); B. Moore *et al.*, Mon. Not. R. Ast. Soc. **310**, 1147 (1999); J.F. Navarro, C.S. Frenk, and S.D.M. White, Astrophys. J. **490**, 493 (1997); *ibid.*, **462**, 563 (1996).

[41] P. Bode, J.P. Ostriker, and N. Turok, astro-ph/0010389, and references therein.

[42] J.J. Dalcanton and C.J. Hogan, astro-ph/0004381; C.J. Hogan and J.J. Dalcanton, Phys. Rev. D **62**, 063511 (2000).

[43] R.A.C. Croft, D.H. Weinberg, N. Katz and L. Hernquist, Astrophys. J. **495**, 44 (1998); A. Nusser and M. Haehnelt, Mon. Not. R. Astron. Soc. **313**, 364 (2000); P. McDonald *et al.*, Astrophys. J. **543**, 1 (2000); M. Zaldarriaga, L. Hui and M. Tegmark, astro-ph/0011559.

[44] R.A.C. Croft *et al.*, astro-ph/0012324.

[45] R.A.C. Croft, W. Hu and R. Davé, Phys. Rev. Lett. **83**, 1092 (1999).

[46] S.S. Gerstein and Ya.B. Zeldovich, Zh. Eksp. Teor. Fiz. Pis'ma Red. **4**, 174 (1966); R. Cowsik and J. McClelland, Phys. Rev. Lett. **29**, 669 (1972).

[47] M. Kawasaki, K. Kohri and N. Sugiyama, Phys. Rev. D **62**, 023506 (2000).

[48] G.F. Giudice, E.W. Kolb and A. Riotto, hep-ph/0005123.

[49] G.F. Giudice, E.W. Kolb, A. Riotto, D.V. Semikoz and I.I. Tkachev, hep-ph/0012317.

[50] S. Burles, private communication.

[51] Sloan Digital Sky Survey, http://www.sdss.org; B. Margon, astro-ph/9805314.

[52] K. Kang and G.S. Steigman, Nucl. Phys. **B372**, 494 (1992).

[53] R.J. Scherrer, Mon. Not. R. Ast. Soc. **205**, 683 (1983).

[54] S. Esposito, G. Mangano, G. Miele, and O. Pisanti, JHEP **09**, 038 (2000); M. Orito, T. Kajino, G.J. Mathews, and R.N. Boyd, astro-ph/0005446.

[55] S. Hannestad, Phys. Rev. Lett **85**, 4203 (2000); J. Lesgourgues and S. Pastor, Phys. Rev. D **60**, 103521 (1999).

[56] I. Affleck and M. Dine, Nucl. Phys. **B249** 361 (1985).

[57] W. Buchmüller and M. Plümacher, Phys. Rept. **320**, 329 (1999).

[58] A.D. Dolgov, D.P. Kirilova, J. Moscow Phys. Soc. **1**, 217 (1991); A.D. Dolgov, Phys. Repts. **222**, 309 (1992); J.A. Casas, W.Y. Cheng, and G.B. Gelmini,

Nucl. Phys. **B538**, 207 (1999).

[59] R. Foot, M.J. Thomson, and R.R. Volkas, Phys. Rev. D **53**, 5349 (1996).

[60] X. Shi, Phys. Rev. D **54**, 2753 (1996).

[61] W.C. Haxton, in *Neutrinos in Physics and Astrophysics: from* 10^{-33} *to* 10^{28} *cm*, ed. P. Langacker (World Scientific, Singapore, 2000), nucl-th/9901076; A.B. Balantekin and W.C. Haxton, in *Proceedings of the 1998 Australian National University Nuclear Physics Summer School*, ed. S. Kuyucak, nucl-th/9903038.

[62] G.M. Fuller, in *Current Aspects of Neutrino Physics*, ed. D.O. Caldwell, (Springer-Verlag, Berlin, 2000).

[63] G.M. Fuller, R.W. Mayle, J.R. Wilson, D.N. Schramm, Astrophys. J. **322**, 795 (1987)

[64] D. Nötzold and G. Raffelt, Nucl. Phys. **B307**, 924 (1988).

[65] M.J. Savage, R.A. Malaney and G.M. Fuller, Astrophys. J. **368**, 1 (1991).

[66] J. Bernstein, *Kinetic Theory in the Expanding Universe*, (Cambridge Univ. Press, New York, 1988).

[67] E. Kolb and M. Turner, *The Early Universe* (Addison-Wesley, Reading, MA 1990), and references therein.

[68] A.D. Dolgov and S.H. Hansen, hep-ph/0009083.

[69] A.D. Dolgov, hep-ph/0006103.

[70] Y. Qian and G.M. Fuller, Phys. Rev. D **52**, 656 (1995).

[71] A.D. Dolgov, Yad. Fiz. **33**, 1309 (1981) [Sov. J. Nucl. Phys. **33**, 700 (1981)].

[72] A. Harris and L. Stodolsky, J. Chem. Phys. **74**, 2145 (1981); *ibid.*, Phys. Lett. **B116**, 464 (1982).

[73] G. Sigl and G. Raffelt, Nucl. Phys. **B406**, 423 (1993).

[74] B.H.J. McKellar and M.J. Thomson, Phys. Rev. D **49**, 2710 (1994).

[75] L. Stodolsky, Phys. Rev. D **36**, 2273 (1987).

[76] R. Foot and R.R. Volkas, Phys. Rev. D **55**, 5147 (1997).

[77] P. Di Bari, P. Lipari, and M. Lusignoli, Int. J. Mod. Phys. **A15**, 2289 (2000).

[78] R.R. Volkas and Y.Y.Y. Wong, Phys. Rev. D **62**, 093024 (2000); K.S.M. Lee, R.R. Volkas, and Y.Y.Y. Wong, *ibid.*, 093025 (2000).

[79] B. Misra and E.C.G. Sudarshan, J. Math. Phys. **18**, 756 (1977).

[80] P. Gondolo and G. Gelmini, Nucl. Phys. **B360**, 145 (1991), and references therein.

[81] R. Barbieri and A.D. Dolgov, Phys. Lett. **B237**, 440 (1990); K. Kainulainen, Phys. Lett. **B244**, 191 (1990).

[82] K. Abazajian and G.M. Fuller (in preparation).

[83] W.C. Haxton, Phys. Rev. D **35**, 2352 (1987).

[84] J.R. Bond, G. Efstathiou, and J. Silk, Phys. Rev. Lett. **45**, 1980 (1980).

[85] F. Boehm and P. Vogel, *Physics of Massive Neutrinos*, (New York, Cambridge University Press, 1987); V. Barger, R.J.N. Phillips, and S. Sarkar, Phys. Lett. **B352**, 365 (1995); **B356**, 617(E) (1995).

[86] P.B. Pal and L. Wolfenstein, Phys. Rev. D **25**, 766 (1982).

[87] D.A. Dicus, E.W. Kolb, and V.L. Teplitz, Astrophys. J. **221**, 327 (1978).

[88] A. Comastri, G. Setti, G. Zomorani, and G. Hasinger, Astron. Astrophys. **296**, 1 (1995); D.E. Gruber, in *X-Ray Background*, ed. X. Barcons and A.C. Fabian, (Cambridge, Cambridge Univ. Press, 1992).

[89] A.E. Hornschemeier *et al.*, astro-ph/0101494.

[90] K. Abazajian, G.M. Fuller, and M. Patel, in preparation.

[91] I.M. Gioia, astro-ph/0010059.

[92] S. Hannestad and G. Raffelt, Phys. Rev. D. **59**, 043001 (1999).

[93] P. de Bernardis *et al.* (BOOMERanG Collaboration), Nature **404**, 955 (2000); A. Balbi *et al.* (MAXIMA Collaboration), Astrophys. J. **545**, L1 (2000).

[94] R.E. Lopez, S. Dodelson, A. Heckler, and M.S. Turner, Phys. Rev. Lett. **82**, 3952 (1999).

[95] G. Steigman, D.N. Schramm and J.E. Gunn, Phys. Lett B **66**, 262 (1977).

[96] K. Abazajian, G. M. Fuller and X. Shi, Phys. Rev. D **62**, 093003 (2000).

[97] E. Lisi, S. Sarkar and F.L. Villante, Phys. Rev. D **59**, 123520 (1999).

[98] See K. Jedamzik, Phys. Rev. Lett. **84**, 3248 (2000), and references therein.

[99] S. Burles and D. Tytler, Astrophys. J. **499**, 699 (1998); **507**, 732 (1998); J.M. O'Meara *et al.*, astro-ph/0011179.

[100] V.V. Smith, D.L. Lambert, and P.E. Nissen, Astrophys. J. **506**, 405 (1998); *ibid.*, **408**, 262 (1993); L.M. Hobbs and J.A. Thorburn, *ibid.* **491**, 772 (1997); R. Cayrel *et al.*, Aston. Astrophys. **343**, 923 (1999).

[101] S.L. Shapiro and S.A. Teukolsky, *Black Holes, White Dwarfs, and Neutron Stars: The Physics of Compact Objects* (Wiley-Interscience, New York, 1983).

[102] H.A. Bethe, Rev. Mod. Phys. **62**, 801 (1990).

[103] H.A. Bethe and J.R. Wilson, Astrophys. J. **295**, 14 (1985).

[104] B.S. Meyer *et al.*, Astrophys. J. **399**, 656 (1992); S.E. Woosley *et al.*, Astrophys. J. **433**, 229 (1994); K. Takahashi, J. Witti, and H.-T. Janka, Astron. Astrophys. **286**, 857 (1994).

[105] R.C. Duncan, S.L. Shapiro, and I. Wasserman, Astrophys. J. **309**, 141 (1986); Y.-Z. Qian and S.E. Woosley, Astrophys. J. **471**, 331 (1996); R.D. Hoffman, S.E. Woosley, and Y.-Z. Qian, Astrophys. J. **482**, 951 (1996).

[106] K.S. Hirata *et al.*, Phys. Rev. Lett. **58**, 1490 (1987); K.S. Hirata *et al.*, Phys. Rev. D **38**, 448 (1988);

R.M. Bionta *et al.*, Phys. Rev. Lett. **58**, 1494 (1987); C.B. Bratton *et al.*, Phys. Rev. D **37**, 3361 (1988); E.N. Alexeyev *et al.*, Pis'ma Zh. Eksp. Teor. Fiz. **45**, 461 (1987) [JETP Lett. **45**, 589 (1987)]; E.N. Alexeyev *et al.*, Phys. Lett. **B205**, 209 (1988).
[107] M. Liebendoerfer *et al.*, astro-ph/0006418; H.-Th. Janka, astro-ph/0008432; A. Burrows *et al.*, Asrophys. J. **539**, 865 (2000); and references therein.
[108] H.A. Bethe, Astrophys. J. **412**, 192 (1993).
[109] H.A. Bethe, G.E. Brown, J. Applegate, and J.M. Lattimer, Nucl. Phys. **A324**, 487 (1979).
[110] G.M. Fuller, Astrophys. J. **252**, 741 (1982).
[111] G.G. Raffelt, *Stars as Laboratories for Fundamental Physics* (University of Chicago Press, Chicago, 1996); G.G. Raffelt, Ann. Rev. Nucl. Part. Sci. **49**, 163 (1999).
[112] M. Patel and G.M. Fuller, in preparation.
[113] G.C. McLaughlin, J.M. Fetter, A.B. Balantekin, and G.M. Fuller, Phys. Rev. C **59**, 2873 (1999); M. Patel and G.M. Fuller, hep-ph/0003034; M. Patel and G.M Fuller (in preparation).
[114] S. Hannestad, H.-T. Janka, G.G. Raffelt, and G. Sigl, Phys. Rev. D **62**, 093021 (2000).
[115] J.F. Beacom, R.N. Boyd and A. Mezzacappa, Phys. Rev. Lett. **85**, 3568 (2000); *ibid.*, astro-ph/0010398.
[116] E.A. Baltz, C. Briot, P. Salati, R. Taillet and J. Silk, Phys. Rev. D **61**, 023514 (2000).
[117] J.N. Bahcall, P.I. Krastev, and A.Y. Smirnov, Phys.Rev. D **62**, 93004 (2000); M.C. Gonzalez-Garcia and C. Peña-Garay, hep-ph/0011245; C.J. Virtue [SNO Collaboration], Nucl. Phys. Proc. Suppl. **87**, 183 (2000); A. Hallin [SNO Collaboration], Nucl. Phys. **A663**, 787 (2000).
[118] L. De Braeckeleer [KamLAND Collaboration], Nucl. Phys. Proc. Suppl. **87**, 312 (2000).
[119] I. Stancu, Nucl. Phys. Proc. Suppl. **85**, 129 (2000);F. T. Avignone and Y. V. Efremenko, **87**, 304 (2000).
[120] K. Nakamura [K2K Collaboration], Nucl. Phys. **A663**, 795 (2000).
[121] P.G. Harris, Nucl. Phys. Proc. Suppl. **85**, 113 (2000); J. Schneps, **87**, 189 (2000).
[122] C. Vignoli *et al.* [ICARUS Collaboration], Nucl. Phys. Proc. Suppl. **85**, 119 (2000).
[123] A. O. Bazarko [BooNE Collaboration], hep-ex/9906003; E. Church *et al.* [BooNE Collaboration], nucl-ex/9706011; MiniBooNE/BooNE Project, http://www-boone.fnal.gov.
[124] R.V. Wagoner, W.A. Fowler and F. Hoyle, Astrophys. J. **148** 3 (1967); L. Kawano, FERMILAB-PUB-92-04-A, Jan 1992.